Growth and Characterization of GaSb Grown from a Split-Sputtering Target

GROWTH AND CHARACTERIZATION OF GaSb GROWN FROM A SPLIT-SPUTTERING TARGET

BY

FOUAD HEJAZI

B.ENG

A THESIS

SUBMITTED TO THE DEPARTMENT OF ENGINEERING PHYSICS

AND THE SCHOOL OF GRADUATE STUDIES

OF MCMASTER UNIVERSITY

IN PARTIAL FULFILMENT OF THE REQUIREMENTS

FOR THE DEGREE OF

MASTERS OF APPLIED SCIENCE

MASTERS OF APPLIED SCIENCE (2014) McMaster University

Department of Engineering Physics Hamilton, Ontario

TITLE: Growth and Characterization of GaSb Grown from a Split-Sputtering Target

AUTHOR: Fouad Hejazi

B.Eng. (Electrical Engineering)

Carleton University, Ottawa, Ontario

SUPERVISOR: Dr. Adrian H. Kitai

PAGES: xi,84

DEDICATED TO MY LOVING AND SUPPORTING FATHER,

Dr. RAMZI HEJAZI

Abstract

GaSb is a semiconductor material having a narrow band gap in the infrared spectrum of 0.72 eV. This research is intended to investigate the low cost growth and properties of GaSb and to propose this material as a candidate for a cost effective method of developing a GaSb /silicon tandem solar cell. This work investigated the sputtering of GaSb films onto a glass substrate from a GaSb/Sb split-sputtering target. A GaSb compound was formed by placing Ga and Sb elements inside a vacuum sealed ampule. The ampule was placed inside a box furnace and heated at 800 ^{0} C successfully forming a GaSb compound. Both GaSb and Sb were molded into a semicircular shape in a quartz container. X-ray diffraction (XRD) was conducted on sputtered films in order to confirm their structure. XRD peaks of the film were compared with reference peaks found on the Inorganic Crystal Structure Database (ICSD). GaSb peaks were apparent at specific sputtering chamber conditions of substrate temperature and source-to-substrate distance. Sputtered GaSb films were then further characterized with the Scanning Electron Microscopy (SEM), Fourier Transform Infrared Spectroscopy (FTIR) and Hall Effect measurements. A theoretical thickness of the films was calculated using FTIR measurements to be about 1 µm and 0.35 µm for the films grown on a substrate heated with heater powers of 280 watts and 250 watts respectively. SEM confirmed the sample thicknesses with 20% error. Hall Effect measurements resulted in a high carrier concentration and low free carrier activation energy; $7.545\ x10^{19}\ cm^{-3}$ and 0.1017 eV respectively. These values are attributed to the possible existence of anti-site defects.

Acknowledgments

I would like to first thank God for the strength and perseverance he has given me to complete a Masters of Applied Science in Engineering Physics. My deepest gratitude to my supervisor, Dr. Adrian Kitai, his guidance, support and encouragement helped me to succeed through the course of my master's degree. I would like to express my deepest and grateful appreciation to my parents, Dr. Ramzi Hejazi and Mona Al Deeb, for providing me with guidance, moral support and eliminating the term "I Give Up" from my dictionary. I would like to thank the staff at the Brockhouse Institute for Materials Research and Center of Emerging Device Technology for their training, guidance and support in analyzing my samples.

I would like to thank my colleagues for their assistance and extra help they provided me. Finally, I would like to acknowledge the Saudi Arabian Government for their financial support in studying abroad.

TABLE OF CONTENTS

LIST OF FIGURES

LIST OF TABLES

Chapter 1: Introduction

1.1 Background information

Everyday harmful gases formed by burning fossil fuels to generate energy enter our earth's atmosphere. Fossil fuels in the forms of coal, oil and gas have been the main source of energy since the industrial revolution [1]. Due to their detrimental impact fossil fuels have on the environment and its limited availability, cleaner and sustainable sources of energy have been developed such as wind and solar. Solar energy appears to be a favorable candidate to countries around the world due to the abundant amount of energy the earth receives from the sun. Solar panels directly convert sunlight into electricity, Germany broke a record by producing over 50 % of its electrical demand using from solar panels in the summer of 2014 [2]. Alongside, countries in the Middle East such as Saudi Arabia and the United Arab Emirates are investing a substantial amount of wealth in establishing a sustainable energy infrastructure [3,4].

The photovoltaic effect was demonstrated by Alexandre-Edmond Becquerel in 1883. Current was generated while light illuminated two electrodes siting inside an acid solution [5]. The area of photovoltaics has developed substantially by participating researcher contributing to the field. In the 1960's solar panels were used specifically for space applications. After a reduction in price per watt achieved by Exxon in the 1970's, solar power has been used in a variety of different power sectors [6].

Single layer solar cells that absorb sunlight such as Gallium Arsenide (GaAs) have achieved an efficiency of about 30% for a single layer under one sun illumination [7]. Concentrated multijunction solar cells had a breakthrough by reaching an efficiency of near 45% at the Fraunhofer Institute for Solar Energy Systems ISE [8].

Solar cells are essentially semiconductors that produce electricity by converting it from sunlight. Incoming photons with sufficient energy excites electrons to a higher energy states. The electron is then directed out of the solar cell with the aid of an external conductor to flow through an external circuit and back into the solar cell. The minimum energy needed to excite the electron into the conduction band (where the electron is now considered to be free) is called the band energy gap.

In today's photovoltaic industry, silicon (Si) is used as the primary semiconductor material in the production of solar cells amongst other semiconductors. This is due to the abundance of silicon and its ease to manufacture. However, one of the significant drawbacks of silicon is its indirect band gap transition. Typically, the aid of lattice vibrations is required to complete the transition of an electron from the valance band to the conduction band. This in turn results in the requirement of a significant cell thickness, approximately 100 microns. The efficiency of a typical silicon solar cell is between 16 -24 %. A plausible attempt to enhance the efficiency of silicon solar cells is the addition of other absorbing layers connected in tandem with the silicon layer.

Silicon has a band energy gap of about 1.12 eV. When translating this into wavelengths silicon has a cut off wavelength of around 1100 nm. Incident photons with an energy level lower than the cut off energy point of silicon would not have the required energy to excite the electron to the conduction band. The remaining energy from an incident photon with a higher energy level than the band gap of silicon is typically wasted and transferred into heat.

Gallium Antimonide's (GaSb) band energy gap is around 0.72 eV. Having a narrow and direct band energy gap, GaSb is optimally operated in the infrared region of the solar spectrum, typically around a wavelength of 1700 nm. This promotes the material to be applied in different long wavelength semiconducting application such as LEDs, photodetectors and solar cells.

1.2 Previous Work on GaSb

Narrow band gap material such as GaSb produces a low open circuit voltage. For that, in the pursuit of developing a high efficiency solar cell narrow band gap semiconductors are more commonly used in multijunction solar cells in attempt to utilize the entire light spectrum [9]. GaSb has been used as a booster cell in previous work [9]. It was mechanically stacked with GaAs producing a two layer multijunction solar cell with an efficiency of approximately 37 % under 500x illumination [10]. GaSb was also attempted to be grown on a silicon wafer via coevaporating Gallium and Antimony from other evaporating sources. This resulted in an efficiency of about 5% under 60mW/cm^2 illumination conditions [10].

1.3 Research Objectives

The main objective of this study is to investigate optical and electrical properties of GaSb grown via Physical Vapor Deposition (Sputtering) onto a glass substrate. For this investigation the following analysis techniques are used to achieve the objective

1) X-ray diffraction is employed to study the crystalline quality and its dependence with the sputtering parameters.
2) Scanning Electron Microscopy (SEM) is used to view grain growth of the samples
3) Hall Effect experiments allow carrier concentration and mobility measurement of the material
4) Fourier Transform Infrared Spectroscopy (FTIR) confirms the refractive index alongside with theoretically calculating its thickness
5) Measuring electron life time assess the quality of the growth

This research is intended to investigate the low cost growth and properties of GaSb and to propose this material as a candidate for a cost effective method of developing a GaSb solar cell/silicon tandem solar cell. The concept is to grow polycrystalline GaSb on to the back contact layer on a transparent silicon solar cell. We use glass in the place of a silicon solar cell because glass allows for the

transmission of a wide wavelength range of light and is less costly for research than transparent silicon solar cells. Not much has been published about the Si/GaSb combination due to its lattice constant. Si solar cells are readily available commercially, and for this reason the aim of this research is to combine the two materials. The approach we are taking is a non-epitaxial approach.

This thesis is organized into 5 chapters. Chapter 2 will discuss how materials are classified, a brief description of the crystal structure of GaSb and its semiconducting electrical and optical properties, basic principles of an operating solar cell and the GaSb solar cell. Chapter 2 will also provide the necessary theoretical background information of the experiments that were undergone; a brief description of Sputtering, the Hall Effect, X-ray diffraction and FTIR are presented. Chapter 3 outlines the experimental set up, sample preparation and experimental procedure. Chapter 4 highlights the results that were obtained alongside their discussion. Chapter 5 includes a summary, conclusion and future work that is recommended.

Chapter 2: Theory

2.1 Basic Physical Properties of Gallium Antimonide

2.1.1 Classification of materials

Studying the electrical property of solids gives rise to materials to be placed in three different categories; conductors, insulators and semiconductors. The classification of these categories is understood from energy bands that are a result from the interaction between electrons and atoms. The higher energy states where mobile electrons may exist is known as the conduction band. The next energy range below this is known as the valance band. The separation between these two bands is referred to as the band gap. Exciting an electron from the valance band to the conduction band to fill available energy states is correlated to the flow of current within a material. Mobil electrons may travel from the valance band to the conduction band by thermal or optical stimulation in the presence of empty energy states as seen in figure 2.1 [11].

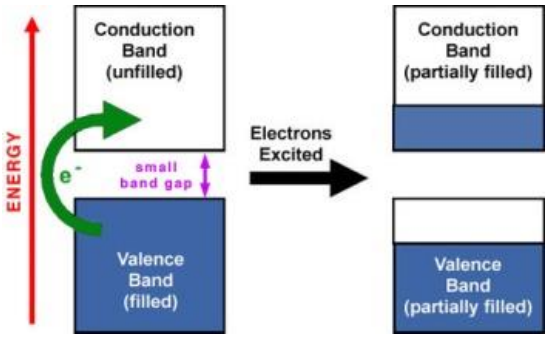

Figure 2.1: Electron Transitioning from Valance band to the Conduction band [12]

In a typical metal the highest occupied states lies within the conduction band creating an overlap region between the valance and conduction band. This in turn eliminates the influence the band gap has on the ability of the electron to transition to the conduction band perming an easy flow of

charge carriers through the material classifying it as a conductor. In the case of semiconductors to overcome an energy gap separation of the two bands the electrons may be stimulated optically or thermally to perform the transition across the band gap. Typically semiconductors have an energy gap separation between less than 1 eV to 3-4 eV [13]. For insulators however, the band gap separation is too large making the transition of the electron from the valance band to the conduction band difficult. Insulators typically have band gaps ranging between 4-6 eV as seen in figure 2.2.

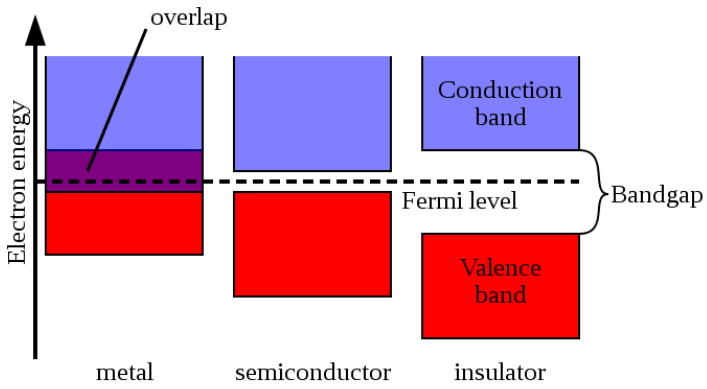

Figure 2.2: Difference in band energy seperation between Metal, Semiconductor and Insulator [14]

2.1.2 Basic Crystal structure of Gallium Antimonide

Gallium Antimonide (GaSb) has a direct energy gap of about 0.72 eV [15]. Direct gap semiconductors eliminate the need for phonons to allow the transition of the electron from the valance band to the conduction band.

GaSb naturally crystalizes in what is known as a zinc-blend structure. The atoms in the crystal lattice align themselves in a way where each atom has four nearest neighbors of the bonded element, and 12 next nearest neighbors forming a tetrahedron as seen in Figure 2.3 [15,16].

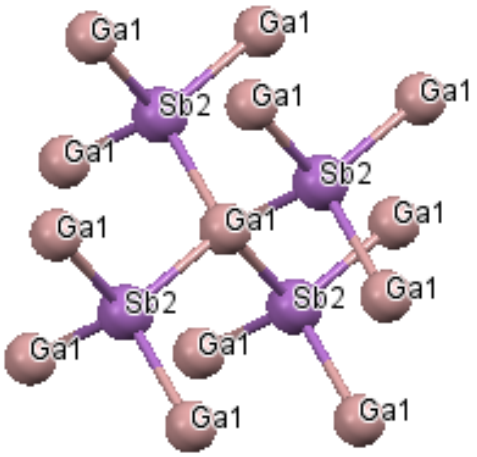

Figure 2.3: GaSb Zincblend crystal structure [17]

Semiconductors with narrow bandgaps typically are used in applications that require the use of longer wavelengths from the electromagnetic spectrum. Taking advantage of GaSb's narrow bandgap to utilize the infrared portion of the electromagnetic spectrum, applications of this semiconductor is seen in laser diodes, photodetectors and tandem solar cells.

2.1.3 Basic Semiconductor Properties

Before tuning the semiconductor to behave appropriately to operate in a desired application, electrical and optical properties of the semiconductor must first be studied.

2.1.3.1 Electrical Properties

2.1.3.1.1 Drift

In the context of semiconductors, Drift refers to the movement of a charged particle in a semiconductor while an external electric field is applied [18]. When an electric field is applied the negative charged particles, electrons, begin to flow in the opposite direction of the electric field. As for

the positive charged particles, holes, they tend to move in the same direction as the electric field as seen in figure 2.4 [18].

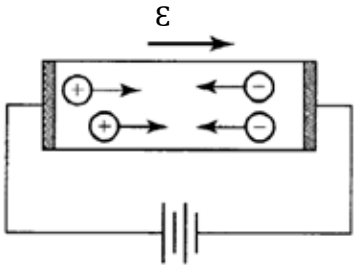

Figure 2.4: Electrons and Holes drift direction with respect to the elctric field [18]

The movement of these charge particles at a certain speed represented as v_d, drift velocity, brings forth the flow of current within the semiconductor. I, the symbol used to represent current, is the charge per unit time. Since the drift current occurs during the presence of an external electric field the drift current is described as the movement of the number of electrons as follows [18]:

$$I_{n|drift} = qnv_dA$$

The drift current due to the movement of the number of holes is as follows [18]:

$$I_{p|drift} = qpv_dA$$

where n and p are the concentration of electrons and holes per unit volume respectively and A is the cross sectional area of the semiconductor. The electric field is what drives the movement of the charge carriers. Expressing this analytically yields an expression for drift velocity v_d and its relationship to the electric field is as follows [18]:

$$v_d = \mu_n \mathcal{E}$$

where μ_n is the electron mobility and Ɛ is the electric field. Incorporating the hole mobility the equation results in as follows [18]:

$$v_d = \mu_p \mathcal{E}$$

where μ_p is the hole mobility and Ɛ is the electric field.

2.1.3.1.2 Mobility

Mobility refers to the ease of movement of a charge particle within a material. The mobility of a charge particle is essential when electrically characterizing a material. Studying this property gives an insight to how charge particle behave within a material which in turn results in information of how conductive a material is [18].

Describing conductivity analytically results to the following equation [18]:

$$\sigma = q(\mu_n n + \mu_p p)$$

where q is the charge in Coulombs, μ_n is the electron mobility, n electron carrier concentration, μ_p is the hole mobility and is p is the concentration of holes [18].

A very significant factor that affects mobility is the amount of scattering that charge carriers undergo within the semiconductor. If the amount of scattering that takes place within the semiconductor is significantly large, the mobility of the material is decreased. Prime mechanisms of scattering include phonons or the existence of impurities and defects. Phonons refer to the vibrations that take place within the lattice due to thermally excited atoms within the lattice [18]. If the amount of vibration is increased the probability of charge carriers colliding with the vibrating lattice will increase which in turn results in an increase of scattering and a decrease in mobility.

Another mechanism that permits the scattering of charge carriers is the coulombic force of attraction or repulsion between the charge carriers and ionized donors or acceptors. Impurities that exist naturally within a semiconductor as well as defects promote scattering and the decrease of mobility [18].

2.1.3.2 Optical Properties

2.1.3.2.1 Reflection, Refraction and Transmission

Generally, when light is incident on a plane surface interface, light is reflected off the surface at the same angle as the incident light. Parts of the light propagate through the material slanted at an angle, this is known as Refraction. The angle at which the light bends is due to the refractive index of the media it is travelling through [19] as see in figure 2.5.

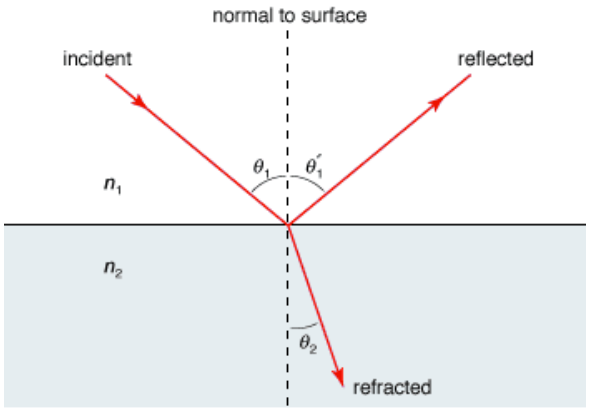

Figure 2.5: Illustration Reflection and Refraction of light [20]

The refractive index of a material is defined by the ratio of the speed of light moving through vacuum to the velocity of light propagating through a material.

$$n = \frac{c}{v}$$

where n is the refractive index of a material, c is the speed of light travelling in vacuum and v is the velocity of light through a medium. Snell's law analytically defines the relationship between the angle of incidence and the direction of the refracted light in media having different refractive indices. If light is transmitted through different media with different refractive indices, Snell's law is as follows [19]:

$$\frac{sin\theta_{incident}}{sin\theta_{refracted}} = \frac{n_{refracted}}{n_{incident}}$$

2.1.3.2.2 Light Absorption, Generation and Recombination of Carriers

Generation refers to the creation of electrons and holes. Carriers may be generated thermally where sufficient thermal energy is absorbed exciting the electron from the valance band to the conduction band. Incident photons with higher energies than the band gap energy of the semiconductor would optically excite electrons causing the generation of charge carriers [18] as see in figure 2.6.

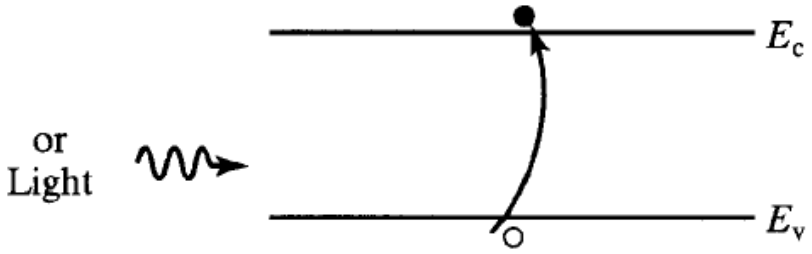

Figure 2.6: Optically generated carriers [18]

Recombination refers to the annihilation and destruction of the electrons and holes. The recombination process could be summed up into two different categories; radiative and non-radiative recombination.

Radiative recombination occurs mostly in direct gap semiconductors where the electron drops in energy from the conduction band to annihilate with a hole in the valance band. The excess energy form the process is released in the form of a photon [18] as seen figure 2.7.

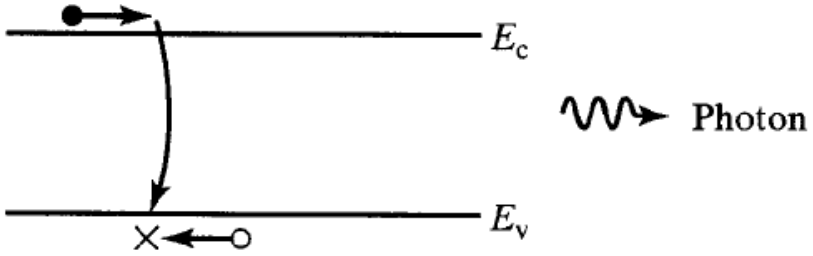

Figure 2.7: Radiative Recombination illustration [18]

In the case of non-radiative recombination, photons are not generated in the recombination process. If the electron does not drop in energy to recombine with hole a photon will not be produced and the excess energy from the annihilation will output as heat or lattice vibration (phonons). The existence of traps often aids the process of recombination. Traps are defects or impurities that exist naturally or are introduced during the growth or treatment process of the semiconductor. If a charge carrier is caught in a trap energy state in the forbidden area, it occasionally forces the freely moving hole (or electron) to recombine with the trapped carrier [18].

In the case of solar cells, electrons flow out of the top front surface of the solar cell, with the aid of an external wire, into the back surface of the solar cell where they often recombine with the holes as seen in figure 2.8. In this case of non-radiative recombination, the electron does not travel from the conduction band to the valance band as it recombines with the hole. This is due to the electron being at a similar energy level as the hole resulting in a non-radiative recombination process.

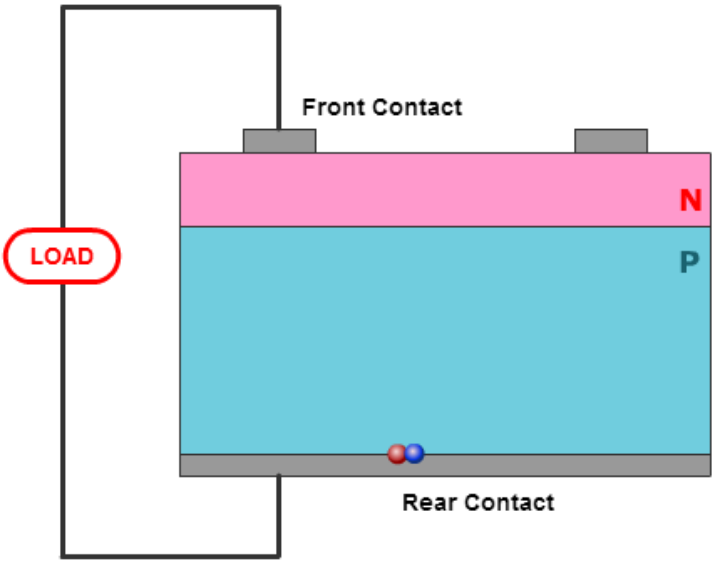

Figure 2.8: Electron and Hole recombine at the rear of the solar cell [21]

Another mean of non-radiative recombination is the Auger recombination process. The auger recombination requires a third charge carrier in the recombination process. When an electron-hole pair recombines and the presence of a third particle is available, the excess energy released from the recombination is transferred to the third charge carrier. The third energized carrier is then excited within the conduction band and loses its energy incrementally by colliding with the crystal lattice. Figure 2.9 illustrates the energy loss of the third electron by the stepping ladder [18].

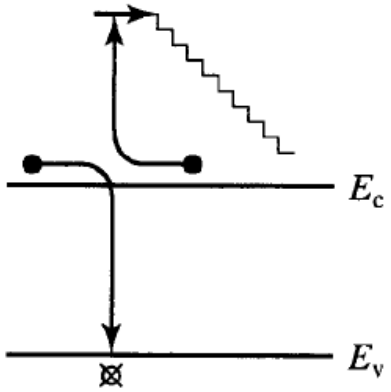

Figure 2.9: Auger Recombination transfer energy degradation [18]

2.2 Multijunction Solar Cells

2.2.1 The solar spectrum

When an object is heated up to a certain temperature it begins to glow and emit radiation, this phenomenon is known as blackbody radiation. At approximately 5500 ^{o}C [13] This type of radiation is the source of light emitting from the surface of the sun giving out an emission spectrum with different wavelengths as seen if figure 2.10. Part of the sunlight entering the earth is absorbed by its atmosphere and scattered throughout the surface of the earth. For that, terrestrial solar cells are designed and tuned to take advantage of the light within the earth's atmosphere.

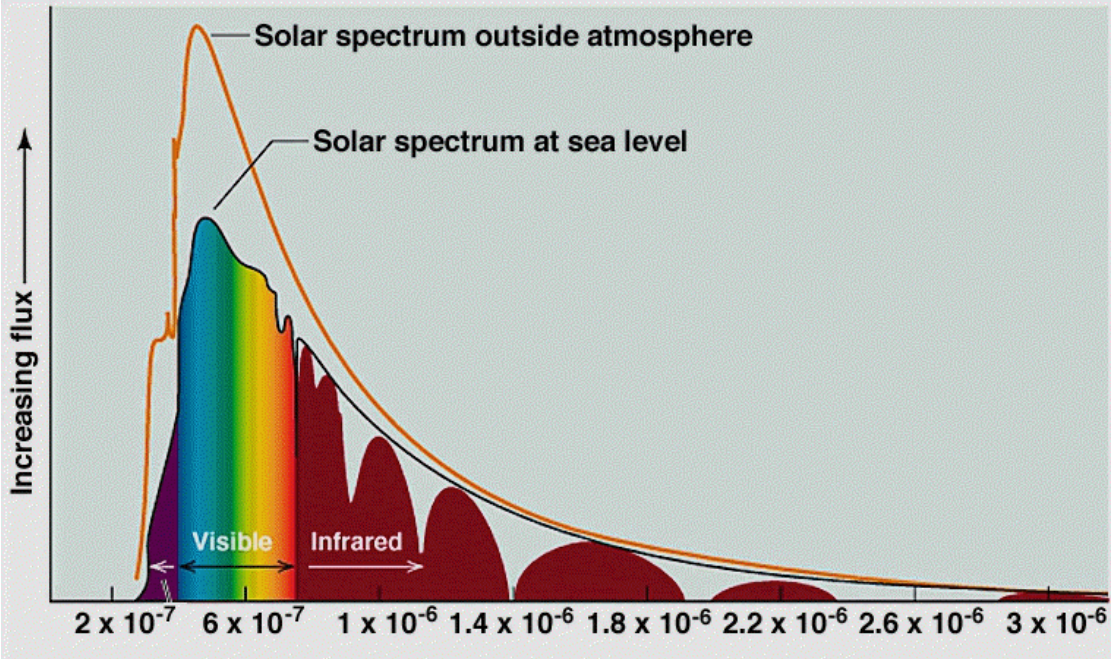

Figure 2.10: Solar spectrum inside and outsid the earth's atmosphere [22]

2.2.2 Basic Principles of Tandem Solar Cells

One of the issues that the single junction solar cells faces is the the overheating due to incident photons with higher energy than the band gap of the cell. A plausible solution to this was the demonstration of the multijunction or a tandem solar cell in 1978 [23]. A multijunction solar cell would

have a number of different solar cells of different energy bands stacked on top of each other to split the solar spectrum. Incident photons of different energy levels are then absorbed by the corresponding solar cell with a similar matched band energy gap. To best utilize this concept, cells of higher energy gaps are placed at the top to absorb the shorter wavelength of light followed by decreasing band energy level gaps to absorb the longer wavelength of light as seen in figure 2.11.

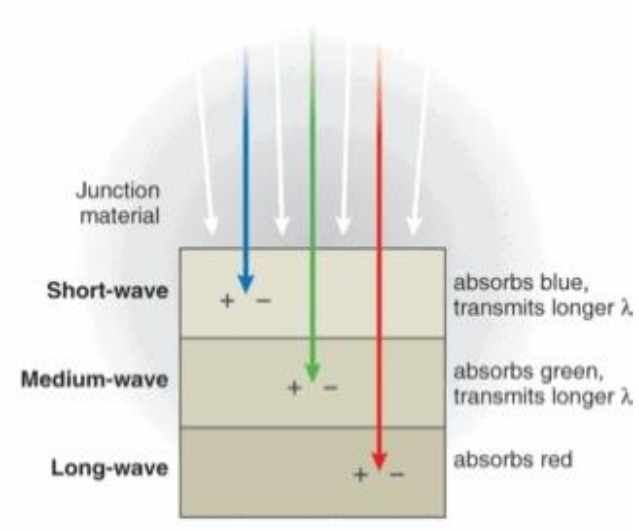

Figure 2.11: shorter wavelengths absorbed by top cell while the longest wavelength is absorbed by the bottom cell [24]

The aim of this particular solar cell design is to utilize the entire light spectrum by absorbing as much of the electromagnetic spectrum as possible, which in turn led to the setting of solar cell efficiency records. Gallium Arsenide (GaAs) single junction solar cells have been demonstrated to hold efficiency records when grown high quality crystals. Its direct energy band gap and its ability to absorb incident photons efficiently all have major contribution to its high efficiency. For that, III-V materials, such as GaAs and GaSb, have been used in fabrication of tandem solar cells.

2.2.3 Physical Properties of Tandem Solar Cells

Tandem cells are either stacked monolithically, each layer grown on top of the other and all under a single substrate, or mechanically, each layer is grown on its own substrate and stacked together

after growth. Challenges do arise when fabricating a tandem cell monolithically such as lattice constant matching and current matching.

2.2.3.1 Lattice Matching

Lattice matching refers to the matching the lattice constants of two or more semiconductors. The lattice constant is the distance between two atoms within the crystal structure. Effectively, the lattice constant is taken into account when growing high quality semiconductors on top of one another. The higher the percentage difference of lattice constants between two semiconductors, the greater the lattice mismatch becomes between the semiconductors which in turn leads to defects in the crystal or high density dislocations which leads to a decrease in the performance of the solar cell [11]. A GaAs/GaSb solar cell combination seems to be attractive due to their band gap range. However, as seen in figure 2.12, GaSb and GaAs have lattice constants of 6.09 Å and 5.56 Å respectively making it difficult to grow high quality monolithic films.

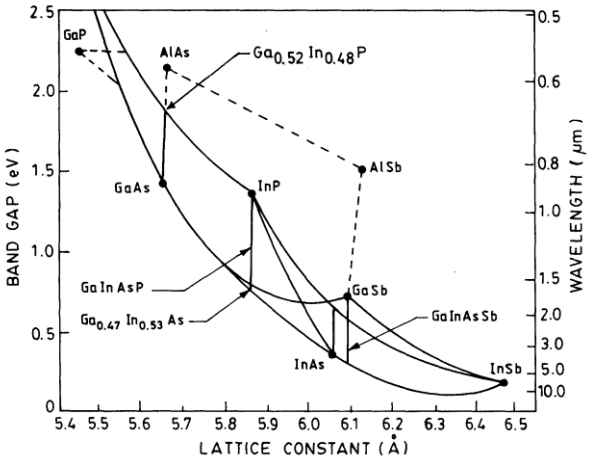

Figure 2.12: Lattice Constant of III-V Materials [15]

2.2.3.2 Current Matching

When cells are stacked monolithically the current of the cell is limited to the lowest current produced by a single cell [25]. The current produced by a solar cell is proportional to the absorption coefficient of a material and its thickness as seen in the equation below. To ensure a steady current flowing through the solar cell the thickness of each layer is calculated and determined based on its particular photon absorption rate.

$$I(x) = I_0 e^{-\alpha x}$$

where $I(x)$ is the radiation intensity propagating through the semiconductor at certain depth of x, I_0 is the radiation intensity at the surface of the semiconductor, α is the absorption coefficient of the material and x is the thickness of the semiconductor[13].

These challenges are avoided when stacking the cells mechanically. The flexibility of design and the use of nearly any desired material does seem beneficial. However, the challenges maintaining the electrical connection and optical configurations far exceed the challenges associated with monolithic stacked cells. For that monolithically stacked cells have had and the most success in improving solar cell performance [25].

2.3 Gallium Antimonide Solar Cells

2.3.1 Gallium Antimonide Basic Band Structure

Gallium antimonide's basic band structure shows a direct energy gap between the valance band maximum and the conduction band minimum of 0.72 eV as seen in figure 2.13.

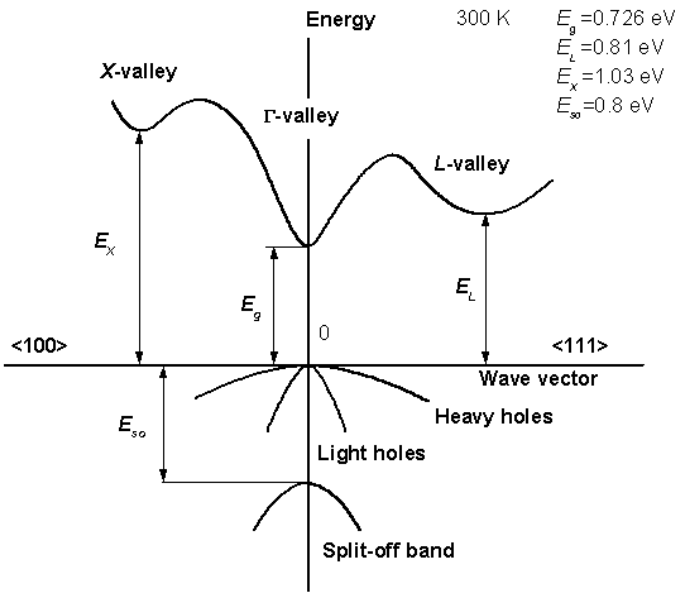

Figure 2.13: GaSb energy band structure [26]

The narrow band gap of the semiconductor allows the material to operate best in the infrared region by analyzing the Planck-Einstein equation:

$$E = \frac{hc}{\lambda}$$

The equation relates the energy of a photon with its wavelength and speed of light where E is the energy of the photon, h is Planck's constant that corresponds to the value of $6.63\ x\ 10^{-34}$ J s. c is the speed of light in vacuum and λ is the wavelength of the travelling photon [13].

Incorporating GaSb's band gap energy into the Planck-Einstein equation:

$$\lambda = \frac{hc/q}{E_{GaSb}}$$

$$\lambda = \frac{6.63\ x\ 10^{-34} J.s\ x\ 3\ x\ 10^{8}\frac{m}{s}/(1.6x\ 10^{-19}\ C)}{0.72\ eV}$$

$$\lambda = 1.727\ 10^{-6} m$$

We see that GaSb has an optimum absorption capability at around 1.7µm that corresponds to the short-wavelength infrared spectrum in the solar spectrum as seen in figure 2.14.

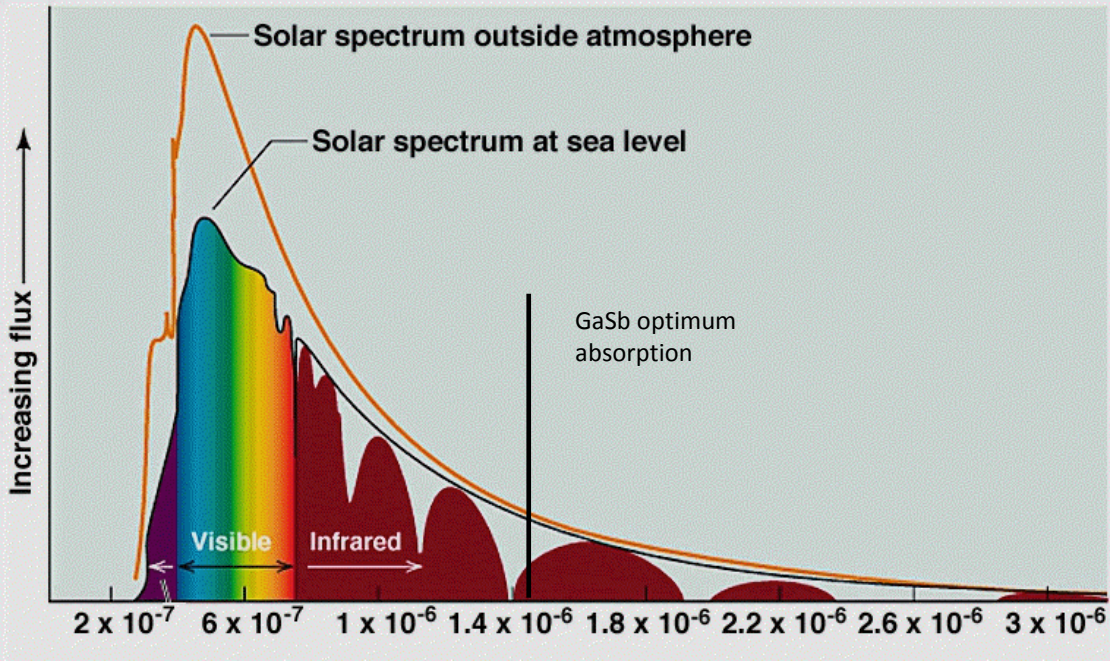

Figure 2.14: indicator showing GaSb optimum absorption wavelength [22]

2.3.2 Basic Properties of Gallium Antimonide p-n Junction

Solar cells are semiconducting materials that are sensitive to light. When creating a solar cell, an intrinsic semiconductor is first put through a process called doping. Doping is the process where impurity atoms are introduced by chemical or physical means to the semiconductor creating an excess of charge carriers, excess of electrons (n-type) or excess of holes (p-type), creating an extrinsic semiconductor. In the case of the compound semiconductors GaSb, it naturally has an excess of donors making it a natural p-type semiconductor. To further increase the acceptor concentration of GaSb elements such as Silicon (Si) or Germanium (Ge) atoms are used to as they are more likely to substitute for Sb atoms creating excess positive [27] charges as seen in figure 2.15.

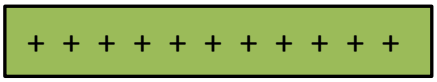

Figure 2.15: P-type layer [Fouad]

To increase donor concentration of GaSb elements such Tellurium (Te), Selenium (Se) or Sulfur (S) atoms are introduced to as they tend to substitute for Ga atoms increasing the donor concentration creating an n-type semiconductor [27] as seen in figure 2.16.

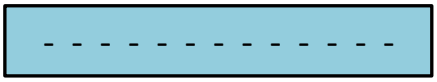

Figure 2.16: N-type layer [Fouad]

When both p-type and n-type semiconductors join together, electrons at the edge of the n-type layer and holes at the edge of the p-type layer start to diffuse and eliminate each other by means of recombination. Instantaneously, an equilibrium state is achieved and a small region depleted from charge carriers called the depletion region is formed as seen figure 2.17 (a). Electrons and holes from the n and p type semiconductors begin to diffuse into the depletion however due to the buildup of an electric field the charge carriers begin to drift in the opposite direction and an equilibrium is maintained as seen figure 2.17 (b). If energy from an incident photon is sufficient in generating an electron-hole pair, they are separated into individual carriers at the junction due to the built in electric field [13].

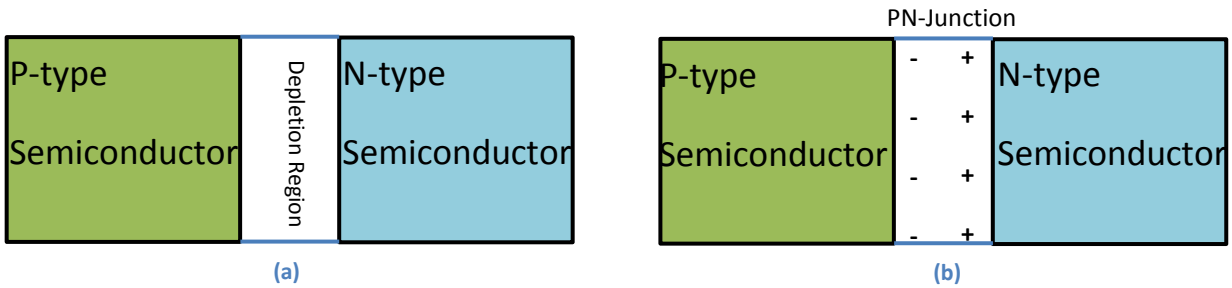

Figure 2.17: (a) Illustration of formation of the depletion region just after bringing the n-type and p-type semiconductor together. (b) Illustration of the formation of the p-n junction where holes drift off to the n-side and electrons drift to the p-side [Fouad]

2.3.3 Gallium Antimonide Tandem Solar Cells

GaSb has been proven through research to enhance the efficiencies of existing solar cells by means of creating a tandem solar cell. GaSb has been demonstrated to increase the efficiency of a Gallium Arsenide (GaAs) solar cell under solar concentration by utilizing the infrared region of the electromagnetic spectrum. GaSb was used to enhance a transparent GaAs solar cell by means of stacking. The overall tandem cell had an efficiency greater than 30% which had set a record at the time [9].

2.4 Brief Theory of Sputtering

The sputtering process is widely used in both industry and in academia. Devices such as solar cells, thin film transistors and LEDS can all be manufactured by sputtering. Alongside thin film deposition, sputtering may also include etching [28]. An advantage that sputtering has over other growth methods is the ability to deposit a film over a large surface area uniformly. This is due to the constant presence of a uniform plasma that is associated with film growth via sputtering. The deposition of poorly conductive materials as well as materials with high melting points is also made possible using sputtering [28]. An overview of sputtering involves atoms being ejected under vacuum from the surface of a source material called the sputtering target. The sputtering target is placed on a metal conductive plate and the film substrate is mounted on an opposing parallel plate as shown in figure 2.18. To begin the deposition process air inside a chamber is evacuated and the pressure is brought down with the aid of vacuum pumps. Sputtering gas is then introduced. Depending on the application of the film, to avoid any chemical reaction between the sputtering gas and the sputtered atoms the sputtering gas is usually an inert gas; generally Argon. Adding the gas in to the chamber raises the pressure inside the chamber to an appropriate growth pressure. An electric field is then applied to excite, accelerate and ionize the gas molecules to create plasma between the two opposing plates. The bombardment of the ionized gas molecules onto the sputtering target causes the atoms on the surface to be ejected and scattered throughout the chamber [28]. Nucleation then begins to occur when atoms make their way onto the

surface of the substrate. The atoms then begin to form clusters of atoms and the desired growth of the film begins to occur [29] as shown in figure 2.19.

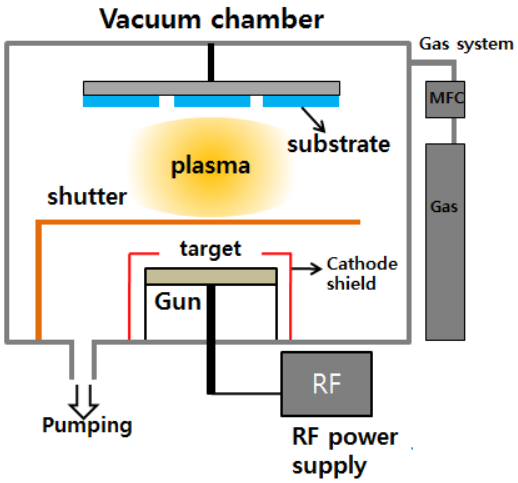

Figure 2.18: Illustration of RF sputtering system [30]

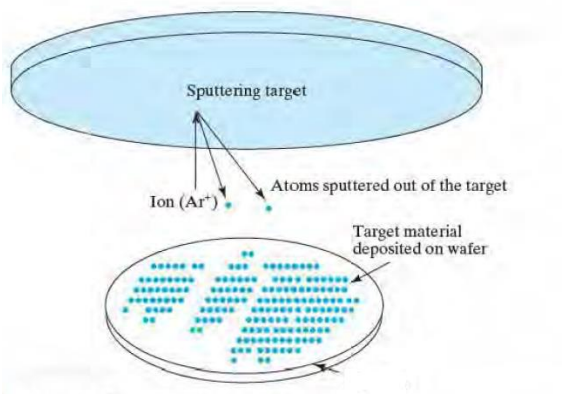

Figure 2.19: Illustration of atoms depositing and nucleating onto a substrate [29]

An advantage that RF sputtering has over DC Sputtering is its ability to sputter using an insulator as a target. If a conductor is used as the sputtering target a constant DC voltage is used to accelerate the ions. Once the ions bombard the target the electrons are able to move freely to avoid any buildup charge. If sputtering using an insulator and DC voltage is present the localized charge will start to build up not allowing any ion bombardment to the surface of the target. In the presence of an RF voltage, the charges are coupled through the target to the bombarding ions. Due to the nature of the RF voltage a negative bias charge is present allowing the target to continually sputter.

2.5 Hall Effect

The Hall Effect is a phenomenon discovered by Edwin Hall in 1879. Applying a magnetic field perpendicular to moving charge carriers, a force is exerted allowing the charge carriers to pile up on the side of the material leaving a net charge of excess electrons on one side and excess holes on the other as shown in figure 2.20. Eventually the edges of the material are saturated with the buildup of charge

particles and current will again flow as it would without the presence of the magnetic field [31]. Measuring the voltage across the edges of the material yields what is known as the Hall Voltage as shown in figure 2.21.

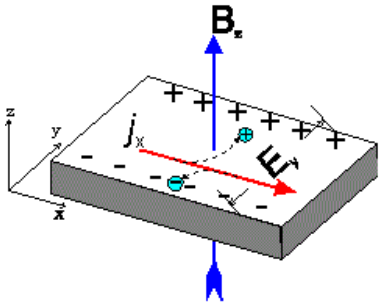

Figure 2.20: charge separation due to presence of magnetic field [32]

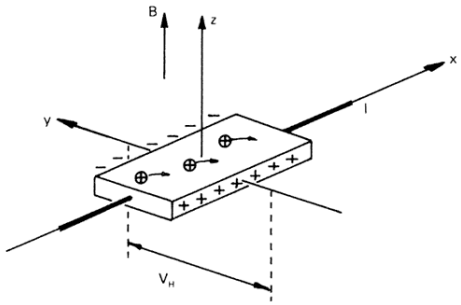

Figure 2.21: Schematic of Hall voltage [33]

Applying Hall Effect measurements the carrier concentration of a sample can be determined by initially finding the hall coefficient [18]. During a steady state current flow through a sample the buildup of charge creates an electric field E_H which in turn gives rise to the transverse electric force -eE_H . Once steady state is reached the transverse electric force is proportional to the product of the drift velocity v_d of the charge carriers multiplied by the transverse magnetic field eB [30].

$$eE_H = ev_dB$$

The hall coefficient is then introduced as R_H as the drift velocity v_d divided by the current density J.

$$R_H = \frac{v_d}{J}$$

An expression for current density J is expressed as the product of electric charge of an electron e multiplied by charge carrier density N_e and the drift velocity v_d.

$$J = -eN_ev_d$$

This in turn leads to an expansion of the Hall Coefficient

$$R_H = \frac{1}{eN_e}$$

2.6 X-Ray Diffraction

In optics diffraction is a phenomenon where incident photons from an electromagnetic radiation source pass through an aperture or multiple apertures small enough to cause the photons to interfere with one another [34]. The interference pattern i.e. diffraction pattern, is then projected and visualized on a screen as shown in figure 2.22. Due to X-rays small wavelengths, 10nm – 0.01 nm, they are found to be ideal to study crystal structures and patterns in the field of crystallography.

Seen in figure 2.23, the diffraction pattern of X-rays reflecting and diffracting off a crystal structure gives an insight and an identity to a material by recording such patterns. The average spacing between atoms alongside with finding the orientation of a particular structure can also be determined using X-ray diffraction.

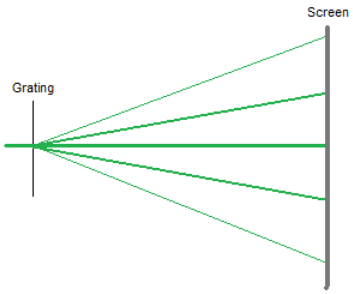

Figure 2.22: Illustration of interference pattern [35]

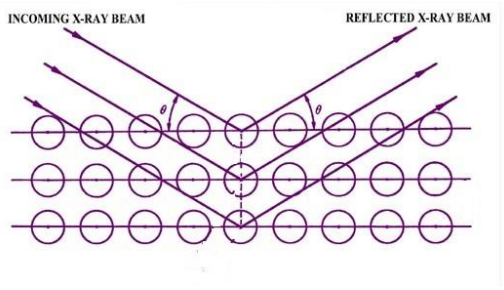

Figure 2.23: X-ray diffraction caused by a crystal lattice [36]

Sir W.H. Bragg and his son Sir W.L. Bragg thoroughly studied the interference patterns produced by X-rays scattered by a crystal lattice to study the atomic spacing and structure of a material. The Braggs were then awarded the Nobel Prize in Physics in 1915 for their work in determining crystal structures by means of X-rays. There work has given rise to what is now known as Bragg's Law, which states an incident X-ray onto the surface of a crystal, its incident angle Θ will reflect back at the same scattering angle Θ. When the path difference, d is equal to the whole number n multiplied by the incident wavelength λ a constructive interference will occur obtaining the following equation:

$$n\lambda = 2d\,sin\theta$$

where n is a whole number, λ is the incident wavelength, Θ is the X-ray incident angle, and d is the crystal lattice spacing.

2.7 Fourier Transform Infrared Spectroscopy

Fourier Transform Infrared Spectroscopy (FTIR) is a method to study the emission or absorption of a material in the infrared part of the electromagnetic spectrum. This type of spectroscopy uses Michelson's Interferometer. An infrared source first strikes a beam splitter the transmitted half of the incident light radiation and reflects the other of half. The transmitted light then strikes a stationary mirror and the reflected light strikes the moving mirror. After reflecting of the respective mirrors, the two light beams recombine at the beam splitter causing a constructive or destructive interference wave, depending on the position of the moving mirror, which is then sent to the sample and a detector detects the amount of transmitted light [37]. The beam is then directed to an IR sensitive detector from which the intensity of light is recorded and plotted in terms of wavenumber as seen in figure 2.24.

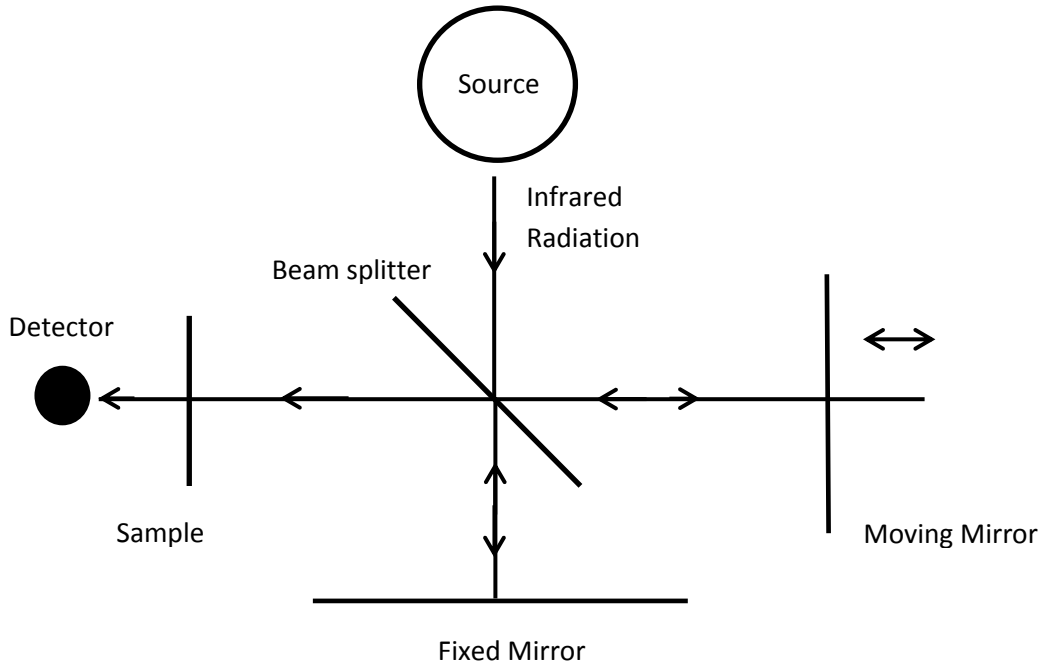

Figure 2.24: Illustration of an FTIR system [37]

As previously mentioned, an incident electromagnetic wave on to a surface of a plane is partially reflected and partially transmitted through the plane. Dealing with two dielectric media with two different refractive indexes the reflection coefficient is given by the following equation [19].

$$R = \left(\frac{n_2 - n_1}{n_2 + n_1}\right)^2.$$

In the case of a thin film GaSb semiconductor deposited on glass, light would have to propagate through three different materials with three different refractive indices as seen in figure 2.25.

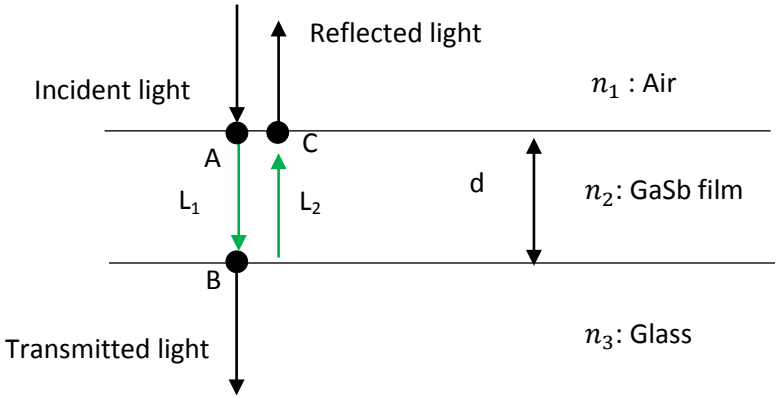

Figure 2.25: Illustration of Optical path through GaSb [Fouad]

As previously mentioned, when light is incident on the surface of a material it is both transmitted and reflected. The transmitted light propagates through the film reflecting off the back surface and traveling through the film once more. As shown in figure 2.25 the incident light is assumed normal to the semiconductor. Marked in green, L_1 propagates through film from point A. The beam is then reflected again inside the film at point B, indicated as L_2, and leaves the film at point C. The optical path difference Δ, in the case of normal incidence, is the addition of the path length of the beams of light traveling inside the film, L_1 and L_2. A film thickness "d' can be calculated by observing the optical path difference resulting in the following equation

$$2d = L_1 + L_2 \,,$$

Or

$$(2d) = \Delta.$$

where Δ is the optical path difference and d is the thickness of the film.

A relative phase shift between the returning light (L_2) and the reflected light occurs at C [19]. The relative phase shift is determined by the thickness of the film and the refractive index of the film. A relative phase shift of multiples of π, (multiples of half a wavelength), causes the beams to interfere either constructively or destructively leading to a maximum or minimum intensity of reflected light. These conditions are:

$$\text{Maxima reflection: } d = \frac{m\lambda_f}{2}, \qquad m = 0,1,2,3,\ldots$$

$$\text{Minima reflection: } d = \left(m - \frac{1}{2}\right)\frac{\lambda_f}{2}, \quad m = 0,1,2,3,\ldots$$

where d is the thickness of the film, λ_f is the wavelength of the light traveling inside the film and is calculated by dividing the light wavelength in air by the index of refraction of the film:

$$\lambda_f = \frac{\lambda_{air}}{n}.$$

An extra phase shift of π at point C is considered due to light arriving from a higher refractive of index (GaSb) to a lower refractive index (air). The conditions of maximum and minimum reflections now become reversed yeilding:

$$\text{Maximum reflection: } d = \left(m - \frac{1}{2}\right)\frac{\lambda_f}{2}, \quad m = 0,1,2,3,\ldots$$

$$\text{Minimum reflection: } d = \frac{m\lambda_f}{2}, \qquad m = 0,1,2,3,\ldots$$

Chapter 3: Experimental Procedure and Setup

A gallium antimonide sputtering target was created to produce a number of GaSb thin films via RF Sputtering. The films were first analyzed by using X-ray diffraction to identify and confirm the nature of the GaSb films. A cross sectional view was taken with electron microscopy to estimate the thickness of the film. Transmission measurements were performed using infrared spectroscopy to study wave interference and to predict and compare the sample's thickness. Metal contacts were sputtered onto the sample and Hall Effect measurements were performed.

3.1 GaSb Sputtering Split-Target

3.1.1 GaSb Split-Target

In order to grow quality GaSb films via sputtering, excess Sb is added to the sputtering target [38]. This is due to the nature of Sb's volatility and high vapor pressure. In previous work [39], a multi-target sputtering system was used as a method of incorporating the required excess Sb into the sputtering target. The targets used were a 1:1 molar ratio of GaSb sputtering-target as the first target and pure Sb as the second sputtering-target. A second approach in growing GaSb films was to incorporate the required excess Sb into a single GaSb sputtering target where a molar ratio of 30% Ga to 70% Sb was demonstrated to be successful [38,39].

For the purpose of this research, we have decided to sputter GaSb films from a split-target. We define our split-target to be a full circular sputtering target split into two halves. The first half consists of a semicircular 1:1 molar ratio GaSb portion, the second half being a semicircular pure Sb portion seen in figure 3.1.

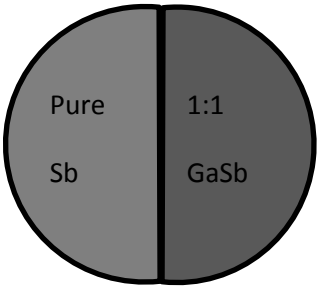

Figure 3.1: GaSb and Sb split Sputtering target schematic [Fouad]

A quartz container glass was made specifically for the project in order to mold our split-target. As seen in figure 3.2 the container is split down the middle allowing the semicircular mold shape to take form. To avoid any contamination and to preserve space, in an inert gas atmosphere tube furnace, half of the crucible was broken off leaving a 2 inch diameter semicircular quartz container for the molding of the split-target.

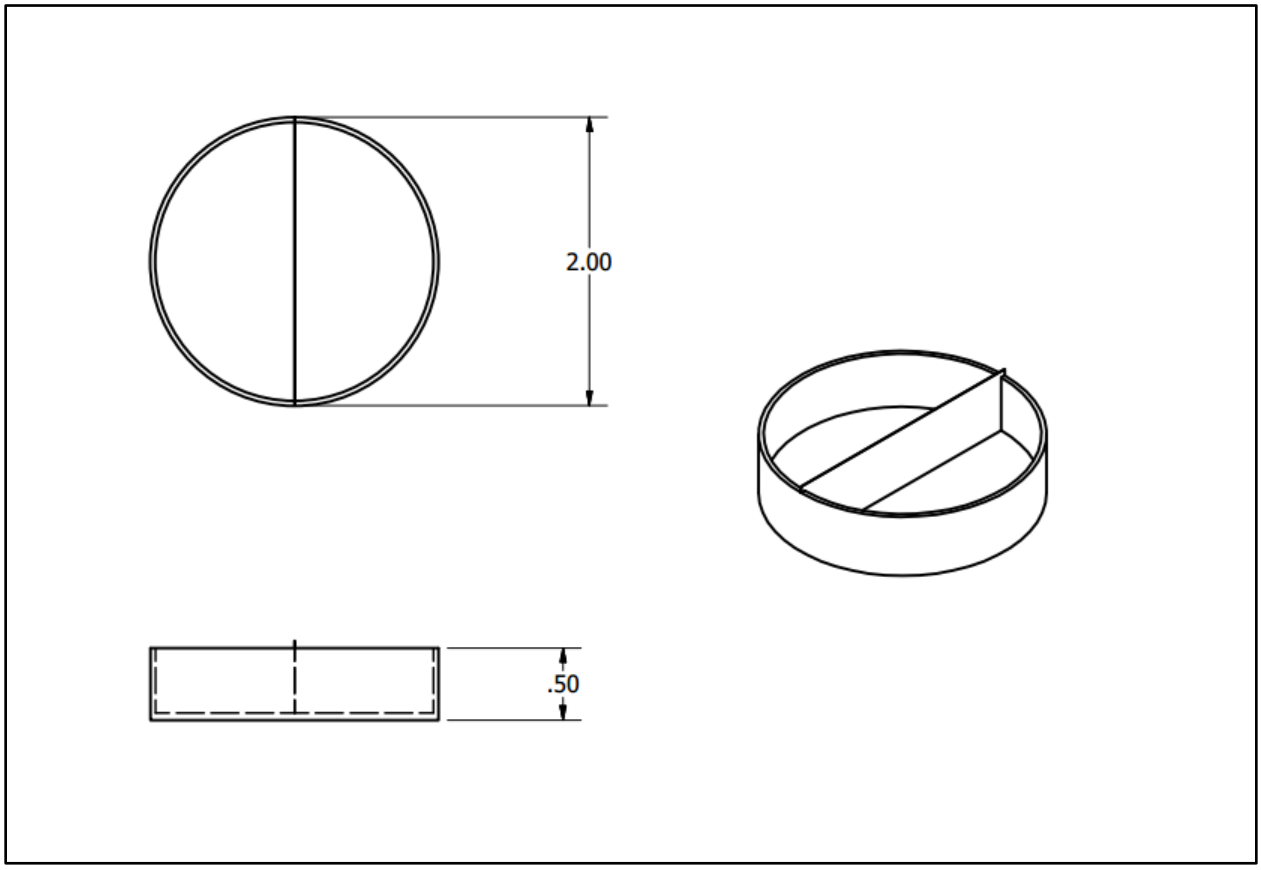

Figure 3.2: Quartz crucible to mold a semicircular target. Units are in inches [Fouad].

3.1.2 Molding GaSb Split-Target

3.1.2.1 Molding Antimony

Antimony shot of a purity percentage of 99.999% was used in forming the first half of the sputtering target. A two inch inner diameter semicircular quartz glass crucible was used to mold the antimony. 48 g of Sb shot was used to fill the quartz crucible. The crucible was placed inside an Argon atmosphere tube furnace set to 800 ^{0}C and left inside for one hour resulting in a slab of Sb molded into a semicircle as seen in figure 3.3.

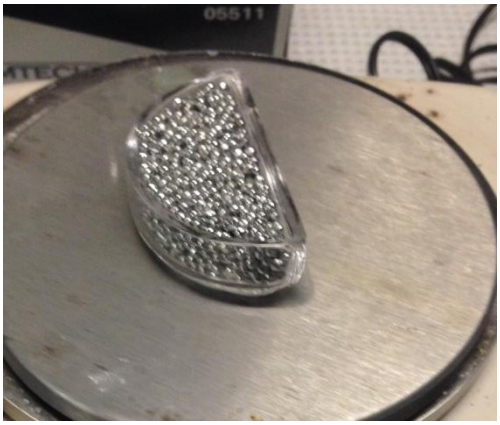

Figure 3.3: (a) Antimony shot inside crucible

3.3 (b) Molded Antimony Shot

3.1.2.1 Molding Gallium Antimonide

As for the GaSb part of the sputtering target multiple attempts went into its making. At first Ga and Sb were placed inside the quartz crucible inside a tube furnace in an argon atmosphere. The sample was successfully molded however due to Sb being denser than Ga, the extra Sb was left unmixed and un-reacted resulting in a molded target with the bottom surface being pure antimony. Attempts to avoid this issue included gently rocking the crucible by twisting the tube of the tube furnace. This method however was unsuccessful and resulted with the same issue alongside the buildup of an oxide

layer on the top surface of the sample. A graphite crucible was also used to replace the glass crucible. However, other issues arose such as the difficulty in removing the sample from the crucible without physically damaging the sample.

Our last attempt to mix gallium and antimony together was with the use of an ampule. Our ampule consisted of a glass tube in which the air was evacuated to a pressure of $2\ x\ 10^{-5}\ torr$. The tube was then sealed with the 1:1 molar ratio of Gallium Antimonide masses inside of it. With this method both the tube furnace and the need for the presence of an inert gas to minimize any oxidation could be eliminated. The ampule was then placed inside a box furnace where is could easily be stirred or agitated avoiding any Sb to be left unmixed as seen in figure 3.4.

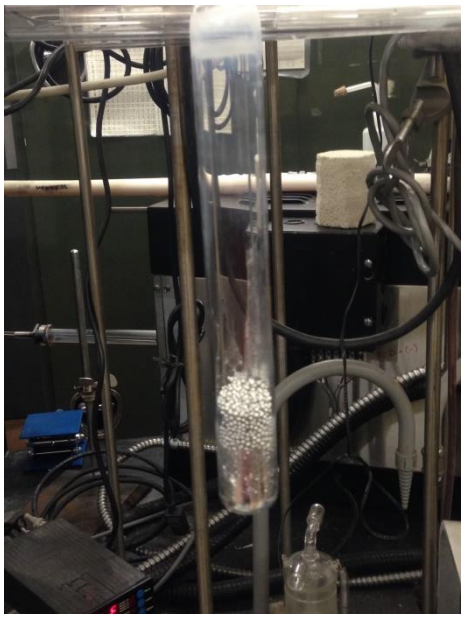

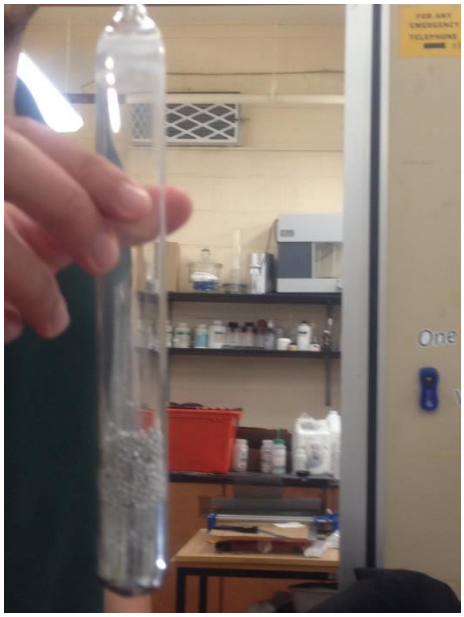

Figure 3.4: (a) Ga and Sb inside the ampule as vacuum is being achieved **3.4 (b) Ga and Sb sealed inside the ampule**

In order to achieve a 1:1 molar ratio of GaSb, 31.01 g of Ga and 54.18 g of Sb were placed inside the ampule prior to sealing. The ampule was sealed and placed inside a box furnace. The temperature

inside the furnace was set to 800 ^{0}C where the ampule was placed inside for an hour. After the hour was over the box furnace was opened and the ampule was agitated using tongs and placed back inside for another 10 minutes. This minimized any Sb settling at the bottom to be left unmixed with the gallium as seen figure 3.5(a) and 3.5(b).

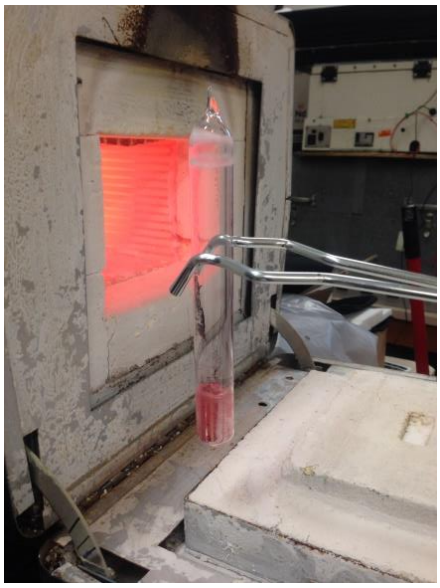

Figure 3.5: (a) Ga and Sb melt inside a box furnace

3.5 (b) stirring the Ga and Sb melt

After the GaSb mixture inside the ampule had solidified, the ampule was broken and the GaSb mixture was removed and placed into the semicircular molding container. The container was placed into the tube furnace for the molding of the GaSb target as seen in figure 3.6.

Figure 3.6: Solid GaSb placed in quartz molding crucible

Once both halves of the target were molded sand paper was used to sand down the split-target creating the necessary surface for the sputtering process to take place, resulting in the final GaSb puttering split-target as seen in figure 3.7.

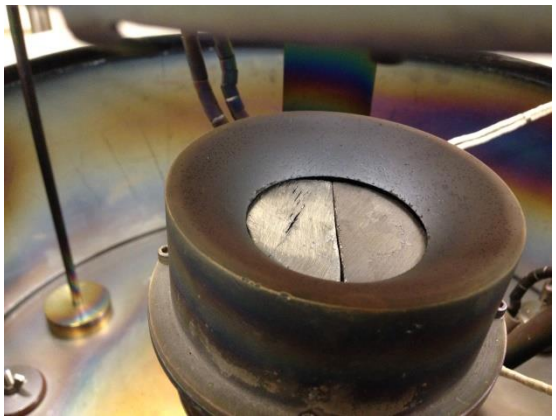

Figure 3.7: Final GaSb sputtering split-target

3.2 Sputtering System Setup

A radio frequency (RF) Sputtering system was provided to grow GaSb films via a sputtering deposition. Argon gas is controlled using a 610A Matheson flow meter. The split- target sits directly on top of the sputtering gun. The sputtering gun is cooled with water from outside of the chamber to avoid

the target from any excessive heating that may impact the growth. The substrate is located vertically above the sputtering split-target, where the heater coils are located directly above the substrate holder plate allowing the substrate to be heated.

Two different setups were used to position the substrate. For the first five growth attempts, a microscope glass slide was used as a substrate and was suspended by clips sitting 5 cm vertically above the sputtering split-target as seen in figure 3.8.

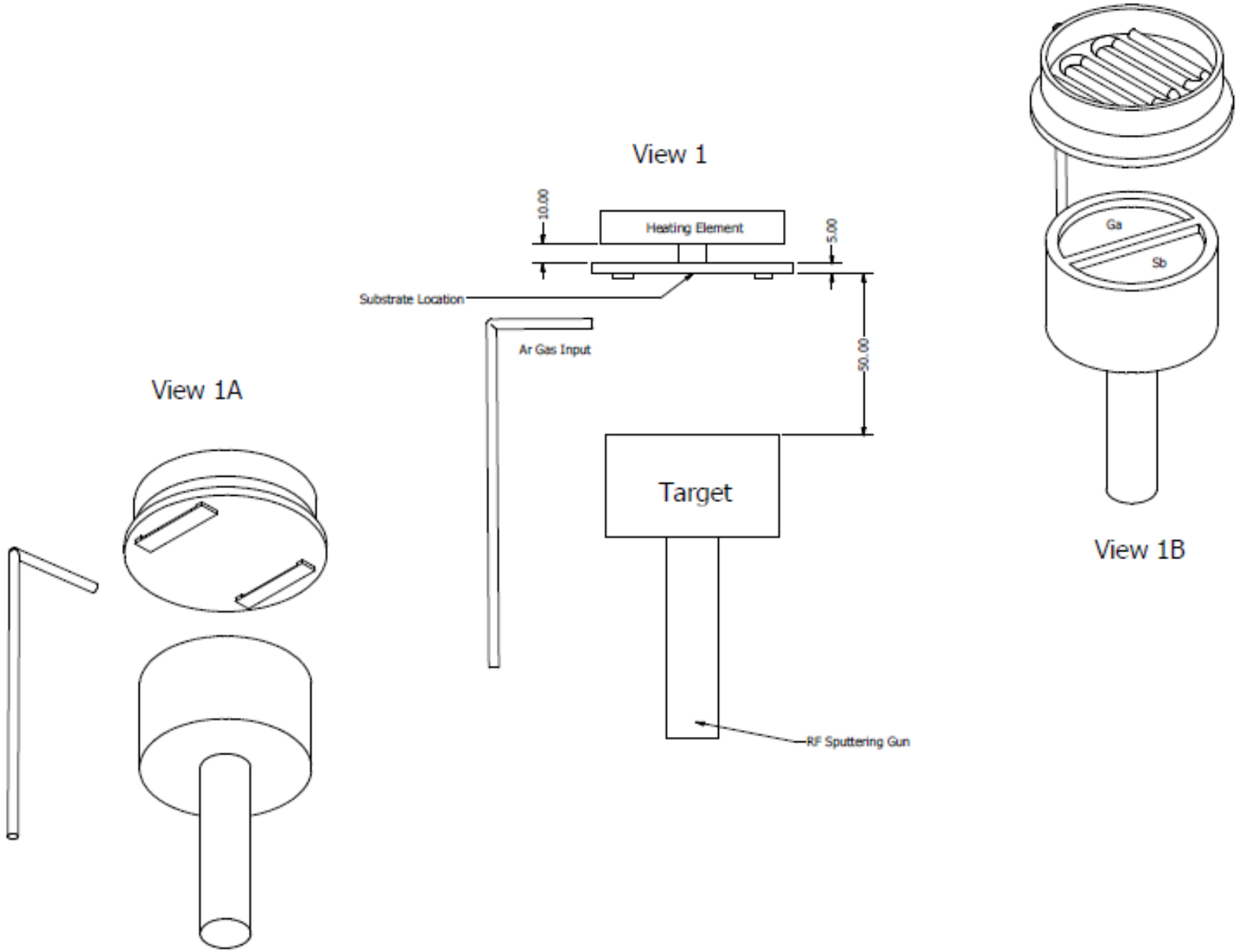

Figure 3.8: Sputtering target setup number 1; target sits 6 cm away from target [Fouad]

Heat from the heater coils was not distributing uniformly throughout the back surface of the substrate, and for this reason the design of chamber was altered.

The second design of the chamber consisted of the substrate to be placed directly touching a metal plate. The plate was placed 1 cm higher yielding a total distance from target to the substrate to be 6 cm above the sputtering split-target as seen in figure 3.9.

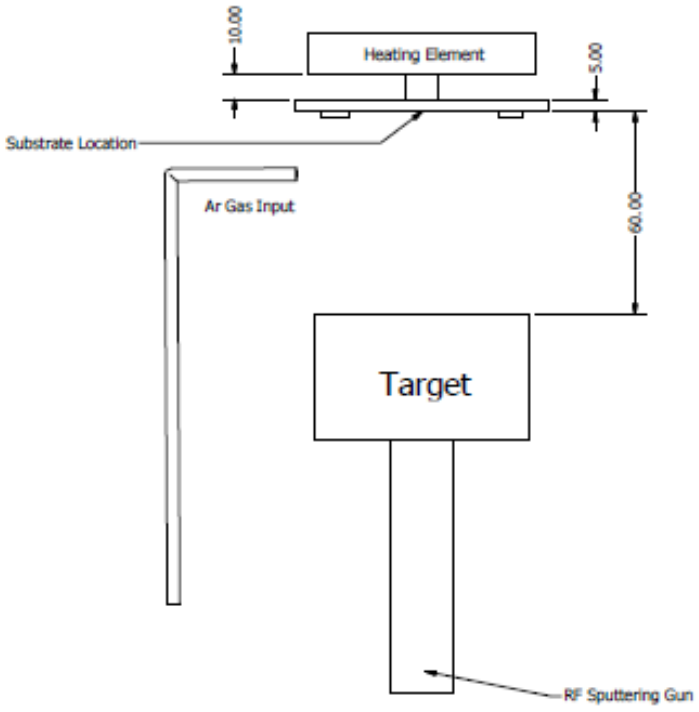

Figure 3.9: Sputtering target setup number 2; target sits 8 cm away from target (units are seen in mm) [Fouad]

The metal plate was secured to the rod with an adaptive locking mechanism. After further unsuccessful growth attempts it was suspected that the cause for this was a result of a hot spot zone located on the substrate. This was due to a direct contact between the rod and the back surface of the substrate. A groove was then machined onto the rod allowing the locking mechanism to secure properly while eliminating the hot spot zone from the substrate. The final GaSb growths were using the same substrate and plate design with the substrate located 5.5 cm above the sputtering split-target.

3.3 Characterization Techniques

A 1 cm x 1 cm sample was sliced and removed from the overall film to further investigate the electrical and optical characteristics of the GaSb films.

3.3.1 Formation of Ohmic Contacts

Provided at McMaster University's Center for Emerging Device Technology (CEDT) a TORR INTERNATIONAL CRC-600 multi target sputtering system was employed. Gold, Au, and Titanium, Ti, sputtering targets were used to sputter ohmic contacts onto a 1 cm x 1 cm sample GaSb film. In past work Ti/Au was demonstrated to be a suitable ohmic contact material for GaSb due to its low resistance contact [40]. Four holes were drilled into a stainless steel sheet to be used as a mask as seen in figure 3.10. The mask was placed directly on top of the GaSb film protecting the surface area of the film from excess Ti/Au during the sputtering process. A total of an approximate 1µm of Ti/Au, 0.12µm of Ti and 0.88µm of Au, was sputtered through the holes of the mask onto the surface of the GaSb film providing the film with its appropriate contacts. The ohmic contacts were then used to further investigate the electrical properties of the sputtered GaSb films.

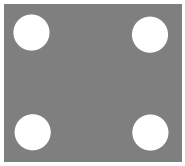

Figure 3.10: Stainless steel mask illustration [Fouad]

3.3.2 X-Ray Diffraction

Results produced by X-ray diffraction (XRD) were observed and compared to powder patterns found on the Inorganic Crystal Structure Database (ICSD). The crystal structure of the grown film species is confirmed by examining the 2-theta scan produced by a diffractometer using both Copper radiation (0.154056 nm) and cobalt radiation (0.179602 nm).

3.3.3 Fourier Transform Infrared Spectroscopy (FTIR)

The thickness of a thin film and its refractive index may be calculated and confirmed respectively by measuring the transmitted light that is incident on its surface. Using Thermo Electron's Nicolet 6700, infrared radiation ranging between 1 µm to 5 µm is incident onto the surface of the film where the percentage of transmitted light is recorded at each wavelength.

3.3.3 Hall Effect Measurements

The Hall Effect measurements were performed using an Ecopia HMS- 3000 Hall Measurment System. The experiments were conducted at room temperature using a 0.55 T magnetic field. The 1 cm x 1 cm sample was place onto the manufacturers sample holder (SPCB-1 Spring Clip Board) and placed inside the HMS-300 where carrier concentration, mobility and resistivity are measured.

3.3.4 Alpha Step Profilometer

The thickness of the thin film may also be measured using an alpha step profilometer. A KLA Tensor Alpha Step D-100 was provided to conduct thickness measurements on a 1 cm x 1 cm sample.

3.3.5 Electron Lifetime Measurements

The minority carrier lifetime was measured using the Photoconductive Decay method. A DC voltage is placed across the sample as a light source near the band gap of the film is incident onto the sample at room temperature. As carriers are being generated, the resistivity of sample decreases and the change in voltage is measured and displayed on an oscilloscope. The circuit setup consists of an input voltage provided by the Hewlett Packard 61217A DC power supply connected in series with a resistor of similar value of the sample. The resistor is connected to a probe that is pinning an ohmic contact connecting the resistor in series with the GaSb film. Another probe is pinning a second ohmic contact that is connected to the DC power supply completing the circuit as seen in figure 3.11. A Tektronix TDS 210 digital real time oscilloscope is used to measure and display the voltage across the sample to measure the change in voltage of the GaSb film as a function of time. An infrared source LED is connected to a 4003 A BK PRECISSION 4MHz function created a timed electrical pulse allowing pulses of light to illuminate to the sample.

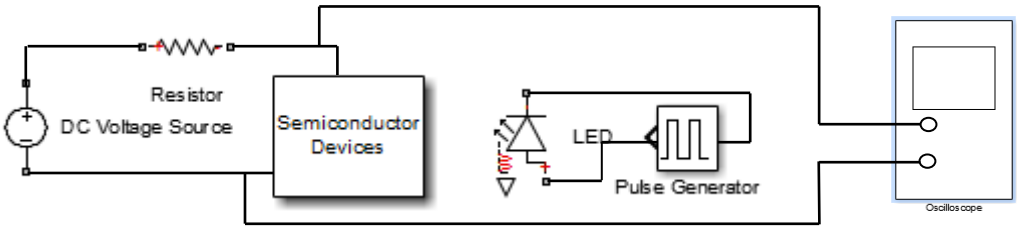

Figure 3.11: Circuit schematic of Photoconductive Decay measurement experiment [Fouad]

Chapter 4: Results and Discussion

GaSb films were sputtered and grown on a glass substrate from an unconventional split sputtering target. Growing and analyzing numerous films demonstrated the success of sputtering a GaSb film from the split target. X-ray diffraction, infrared spectroscopy and electrical characterization all point to the possibility of fabricating a GaSb solar cell.

4.1 X-Ray Crystallography

The crystal structure of both the target and GaSb films were investigated and analyzed using X-ray diffraction. GaSb growth attempts were carried out by Physical Vapor Deposition on a glass substrate from semicircular molded GaSb and Sb targets pieces. X-Ray diffraction was conducted on both the molded split-target and each film grown in an attempt to confirm the materials in the target. Subsequently, the diffraction patterns of the grown films were determined and further electrical and optical investigations were carried out.

Due to the presence of a GaSb split-target, it was hypothesized that a difference in the content of Sb throughout the film would result. As a result of that, the films were categorized into three different categories based on the position of the substrate relative to the target during growth. X-ray diffraction was conducted on all three regions; Sb Poor, Middle Area and Sb Rich. The Sb Poor region was described based on the area of the substrate positioned directly above the GaSb half of the target. In this region of the film, it was hypothesized that X-ray diffraction patterns would result in the lowest content of Sb throughout the film. The Sb Rich is the region described based on the substrate being positioned directly above the Sb region where it was thought to have the highest content of Sb throughout the film. Finally, Middle Area where

the region of the film is located above the center of the GaSb split-target region where an intermediate Sb content was thought to be present.

Numerous growth attempts were conducted in order to determine a suitable growth temperature that would result in a reasonable variation in the content of Sb. The molded split-targets alongside growth attempts 1, 4 and 5 were analyzed using copper radiation (1.54056 Å) as shown in figures 4.1-4.5 respectively. The remaining growths, 6-18, were analyzed using cobalt radiation (1.79602 Å) and these results are seen in figures 4.6- 4.17. The growth parameters of each growth are summarized in tables 4.1-4.13 where a sputtering time of 30 min was employed throughout each growth. The distance between the split-target and the substrate was kept stable between each growth mentioned in chapter 3. The growth temperature varied from each growth to allow the investigation of the crystal structure of the film as a function of temperature. The position of the thermocouple changed during the start of each growth. This in turn led to the conclusion of an unreliable thermocouple reading. Starting from growth attempt 8, the growth temperature was recorded based on the thermocouple readings however, the temperature of substrate was determined using input voltage and hence power of the heating element.

A total of 18 growth attempts were conducted where a total of 13 films were successfully grown. X-ray diffraction patterns of the successful growths were compared to a reference powder pattern found on the Inorganic Crystal Structure Database (ICSD). Reference number 44328 (ICSD) was used as a cross reference check to identify GaSb peaks and reference number 64695 (ICSD) was used as a cross reference check to identify Sb Peaks.

4.1.1: X-ray Results:

The following figures show the X-ray diffraction pattern of each grown film with and its comparison to the reference patterns. From previous work [39] GaSb films seemed to be grown via sputtering at temperatures ranging between 350 ^{o}C to about 500 ^{o}C. The first growth attempt was grown at a recorded temperature of 478 ^{o}C by using the first chamber design mentioned in chapter 3. The thermo couple reading was found to be incorrect due to its position. An adjusted temperature was estimated to be around 300 ^{o}C which resulted in strong peaks of Sb throughout the film which implied a low growth temperature where the excess Sb was not vaporized as seen in figure 4.3. Realizing that the thermocouple was placed far from the substrate, a substrate temperature of about 300 ^{o}C was later to be presumed.

Attempting to grow another GaSb film at a similar temperature as the first growth attempt, the position of the thermocouple was changed for a more accurate estimate of the substrate temperature. The second and third growth attempts were unsuccessful due to equipment complications. The fourth growth attempt resulted in X-ray diffraction patterns of GaSb peaks which did not crystalize in an orderly manner as seen in figure 4.4. This was believed to be a result of the substrate temperature being too hot where the growth conditions are summarized in table 4.2. In an attempt to achieve a crystalline GaSb, during the fifth growth attempt, the substrate temperature was lowered to 330 ^{o} C where the growth conditions are summarized in table 4.2. This resulted in GaSb peaks to be present throughout the film at a preferred orientation at the (2 2 0) direction as seen in figure 4.5.

A Hall Effect measurement of this growth attempt was unsuccessful due to the observation of virtual short circuit when probing the sample with an ohm meter. This is believed

to be a result of anti-sites doping effect taking place throughout the film. For that, the second design of the chamber mentioned in chapter 3 was implemented.

The sixth GaSb growth attempt was grown using the second chamber design where the back of the substrate was flat on a stainless steel plate. The growth conditions mentioned in table 4.4 yielded strong Sb peaks throughout all three regions of the film oriented at the (1 0 -2) direction. A second broader peak oriented at (1 0 4) direction is only seen in two regions of the film. The initial test of probing the film with an ohm meter resulted in a virtual short circuit showing that the film was conductive and Hall Effect measurements could not be performed. As seen in figure 4.7, the seventh growth attempt resulted in a lower intensity X-ray peaks oriented in the same direction as the previous attempt with growth conditions summarized in table 4.5. Due to the volatility of antimony, the observed a lower intensity peaks were thought to be the result of the slight increase in temperature. However, GaSb peaks were not present in the X-ray diffraction pattern and the film gave a virtual short circuit when performing the probe test and Hall measurements could not be performed. Further increasing the growth temperature as seen in table 4.6, growth attempt 8 resulted in a pealed crater located in the center of the film. The peeled section was a result of the metal rod mentioned in chapter 3 touching the back surface of the substrate creating a hot spot zone. X-ray diffraction yielded in higher intensity of Sb peaks in growth attempt 8 than seen in growth attempt 7. This may be attributed to sample 8 being thinner than sample 7 as a result of lower sticking coefficient with the increase in temperature.

Before concluding the hot spot was the cause of the peeling of the sample, growth attempt 9 was performed at a lower temperature as seen table 4.7. High intensity Sb peaks oriented in the (1 0 -2) direction as seen in figure 4.9 were apparent. Due to the low input

voltage, the Sb atoms were not vaporizing and were not allowing the GaSb atoms to form on the film. Sb peaks had high intensity in the Middle Area of the film and a virtual short circuit was seen when performing the probe test. Further decreasing the temperature of the parameters as seen in table 4.8, growth attempt 10 resulted in a resistance value of about 200 kΩ in the Sb poor side, 500 kΩ in the Middle area and 900 KΩ in the Sb Rich side when performing the probe test. However, X-ray diffraction measurements showed an amorphous non-crystalline structure with a small ripple at the (1 0 -2) orientation when comparing it to the powder pattern as seen in figure 4.10. Having achieved an amorphous structure at a low temperature, the voltage heater power was increased to 50 V with a thermocouple reading of 598 ^{o}C. The temperature was chosen due to the achievement of GaSb peaks during growth attempt 5 at a similar heater input power. However, the metal rod touching the back of the substrate resulted in the substrate to split in half and a film to further peel which resulted in a failed growth attempt in sample 11. Realizing that the metal rod was causing poor film growths, the third design of the chamber mentioned in chapter 3 was then applied.

Growth attempt 12 was the first attempt of growing GaSb films using the third chamber design. The metal rod was no longer touching the back surface of the substrate with the distance between the split-target and the substrate was controlled. Employing the conditions mentioned table 4.9, GaSb peaks were not visible and strong Sb peaks were apparent at the (1 0 -2) direction as seen in figure 4.11. The heater input power level was then decreased incrementally for both growths 13 and 14. Keeping the conditions as similar as possible to the previous growths, the Sb X-ray peaks orients at (1 0 -2) showed higher intensity as temperature decreased.

Growth attempt 15 was grown at a higher heater power level and the conditions are summarized in table 4.12. The intensity of the Sb peaks decreased as seen in figure 4.15 and was not apparent in both the Sb Poor and Middle Area of the film. Growth attempt 16 had a higher heater power level with an input of voltage of 60 V and a thermocouple reading of 701 ^{o}C. Which resulted in the substrate bend and an unsuccessful growth attempt. The following growth attempt (growth attempt 17) was grown using the conditions mentioned in table 4.13 resulted in an amorphous crystal structure similar to what was observed during growth attempt 10. However, the apparent ripples were oriented at the (1 1 1) direction, as seen in figure 4. 16, implying the presence of GaSb. Using the probe test to measure the resistance of the film resulted in a virtual short circuit and Hall Effect measurements could not be conducted.

Summarized in table 4.14, growth attempt 18 resulted in apparent GaSb peaks with a preferred orientation in the (1 1 1) direction. As seen in figure 4.18, the peaks intensity decreased as the film was scanned from the Sb Poor area to the Sb Rich. X-ray peaks in the Sb Rich area showed intense peaks belonging to both GaSb and Sb. This is indicative of the presence of a 2-phase crystal structure; one belonging to GaSb and the other to Sb. The initial probe test gave a resistance increasing from about 1 to 4 kΩ throughout the film. A cloudy area of the film was present at the Sb Rich area which gave a virtual short circuit when probing it. This area is believed to cause the presence of the 2-phase x-ray peaks in the Sb Rich region. The presence of the resistance measured by the ohm meter allowed Hall Effect measurements to be conducted at different regions of the film.

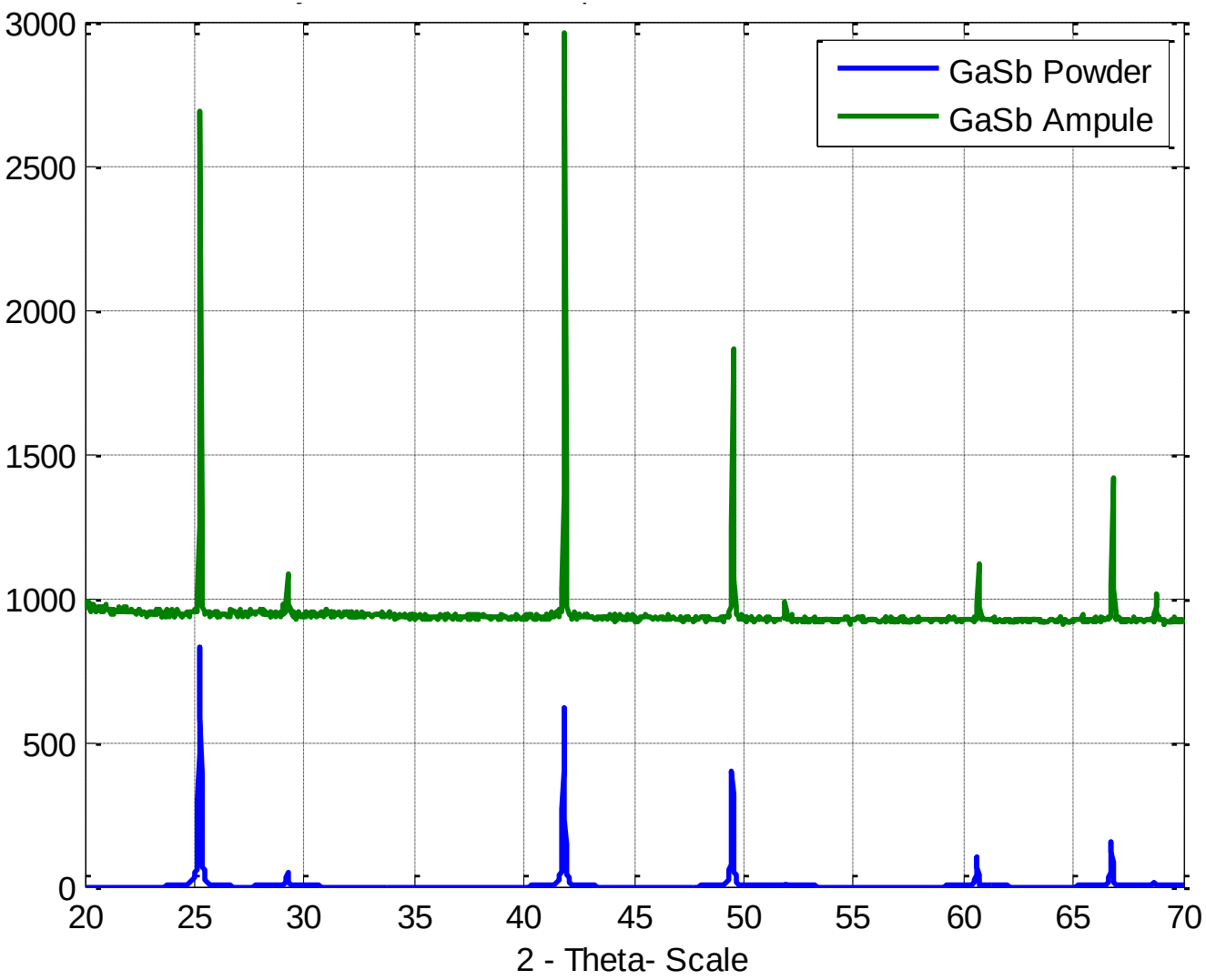

Figure 4.1: X-ray data of GaSb Ampule vs. GaSb Powder Pattern

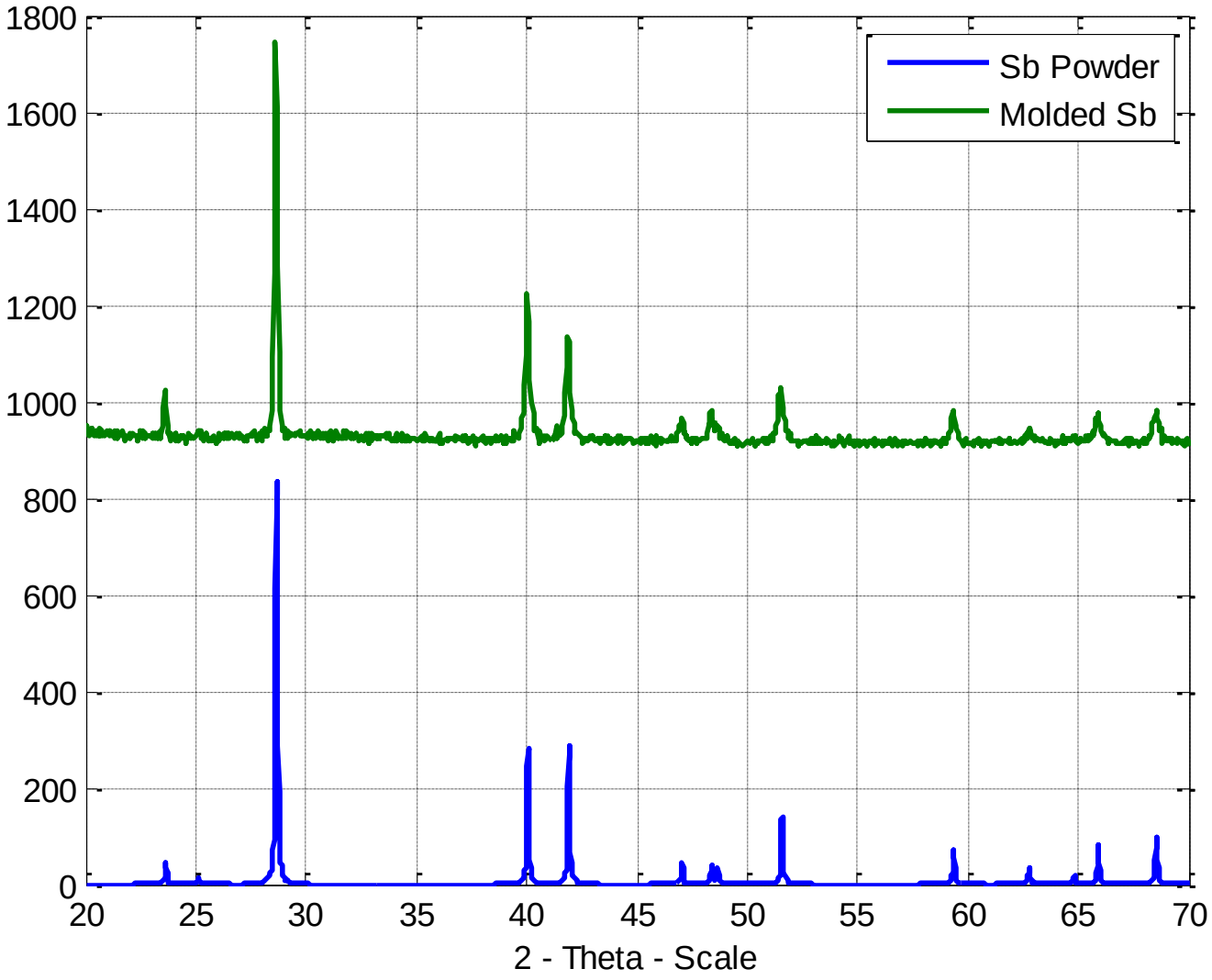

Figure 4.26: X-ray data of molded Sb vs. Sb Powder Pattern

Table 4.1: Growth Conditions of GaSb Growth Attempt 1

Base Pressure	Recorded growth Temperature	Heater Power	Argon Flow Rate	Growth Pressure	Sputtering Power
2.2 x 10^{-5} Torr	478 °C	NA	103 ml/min	10 mTorr	75 Watts

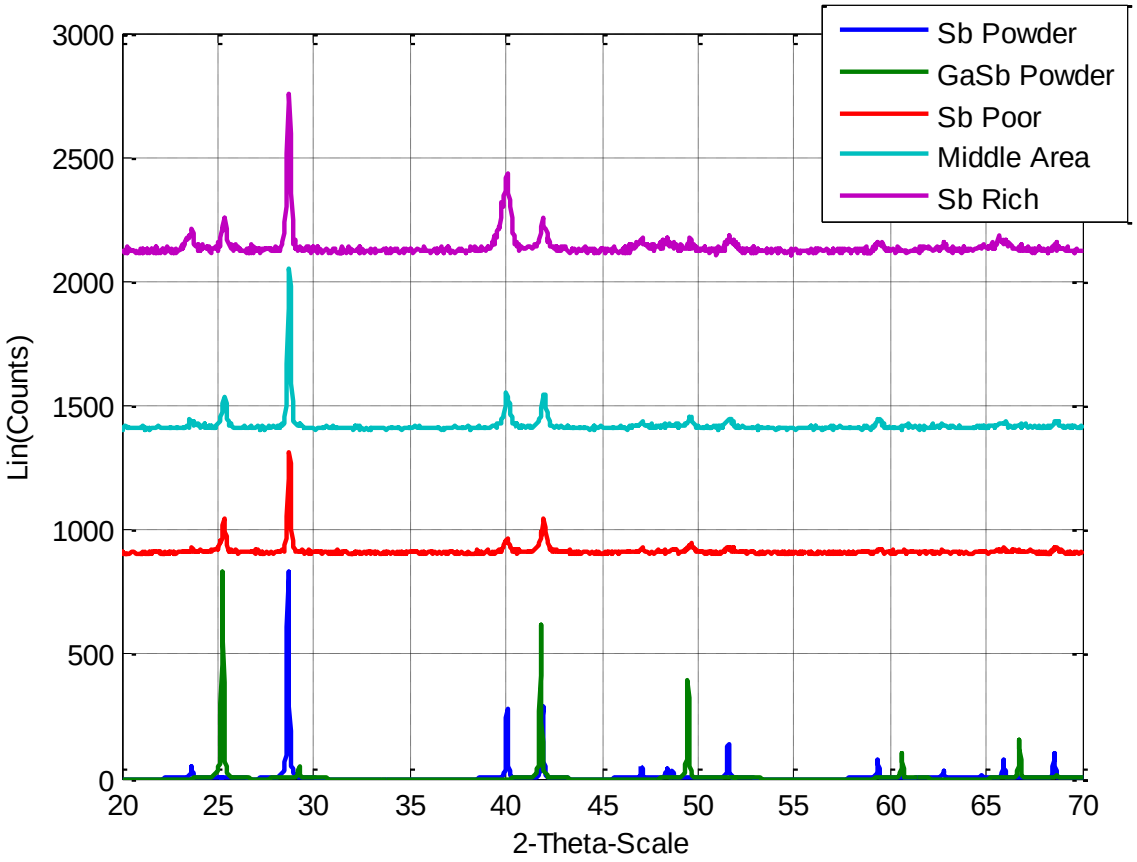

Figure 4.3: X-ray data of GaSb growth attempt 1

Table 4.2: Growth Conditions of GaSb Growth Attempt 4

Base Pressure	Recorded growth Temperature	Heater Power	Argon Flow Rate	Growth Pressure	Sputtering Power
3.4 x 10^{-5} Torr	450 ^{o}C	315 Watts	103 ml/min	10 mTorr	82 Watts

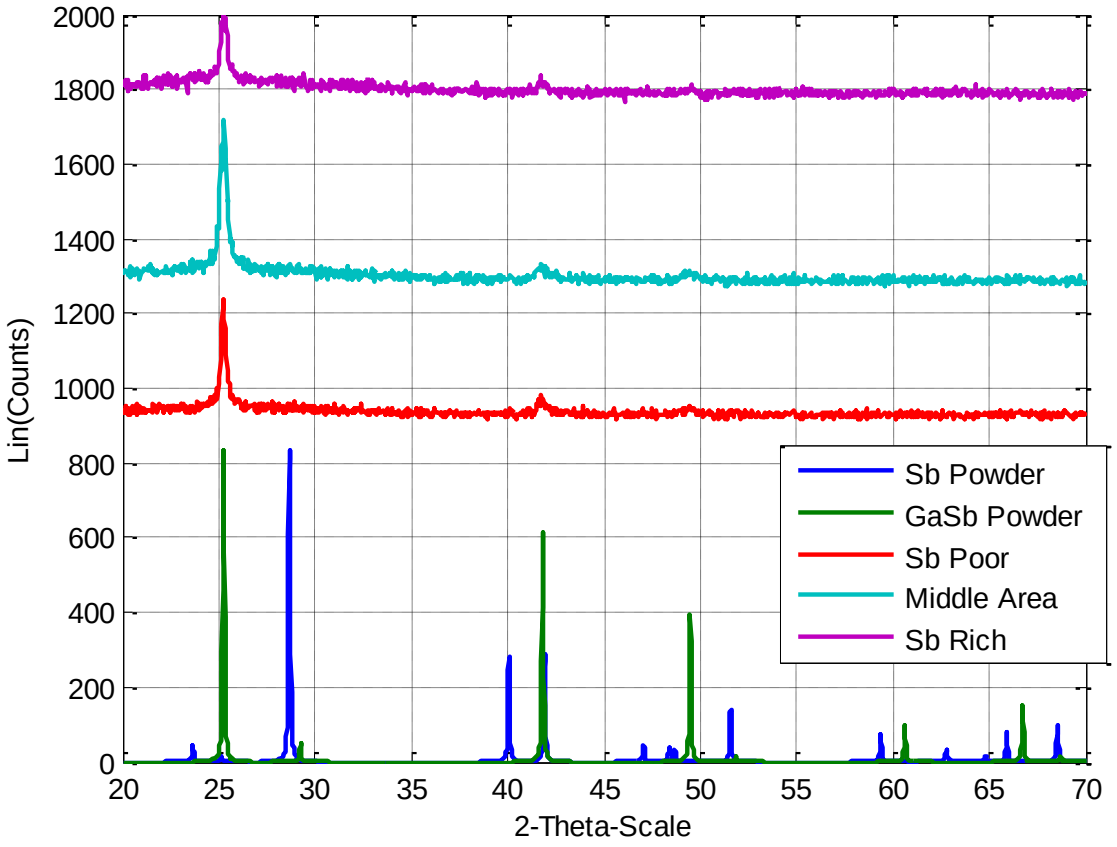

Figure 4.4: X-ray data of GaSb growth attempt 4

Table 4.3: Growth Conditions of GaSb Growth Attempt 5

Base Pressure	Recorded growth Temperature	Heater Power	Argon Flow Rate	Growth Pressure	Sputtering Power
2.2 x 10^{-5} Torr	350 ^{o}C	280 Watts	103 ml/min	8.5 mTorr	70 Watts

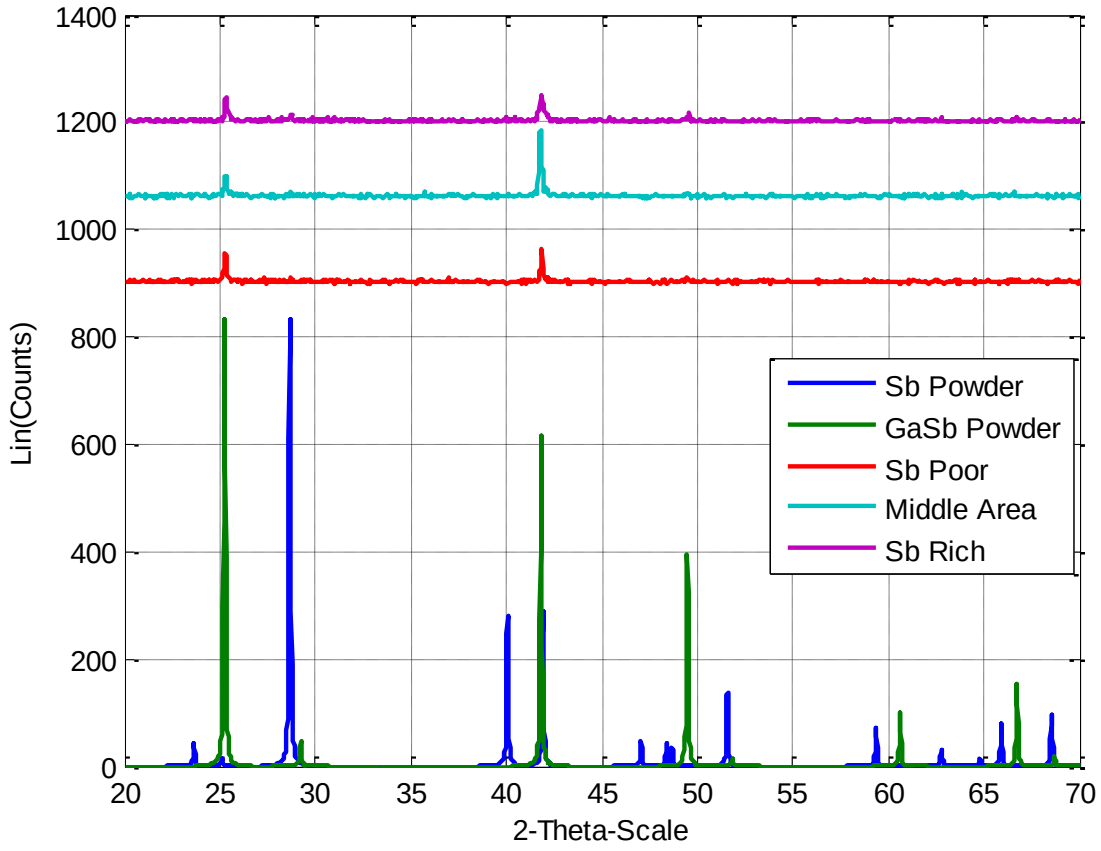

Figure 4.5: X-ray data of GaSb growth attempt 5

Table 4.4: Growth Conditions of GaSb Growth Attempt 6

Base Pressure	Recorded growth Temperature	Heater Power	Argon Flow Rate	Growth Pressure	Sputtering Power
1.9 x 10^{-5} Torr	361 °C	NA	103 ml/min	10.5 mTorr	60 Watts

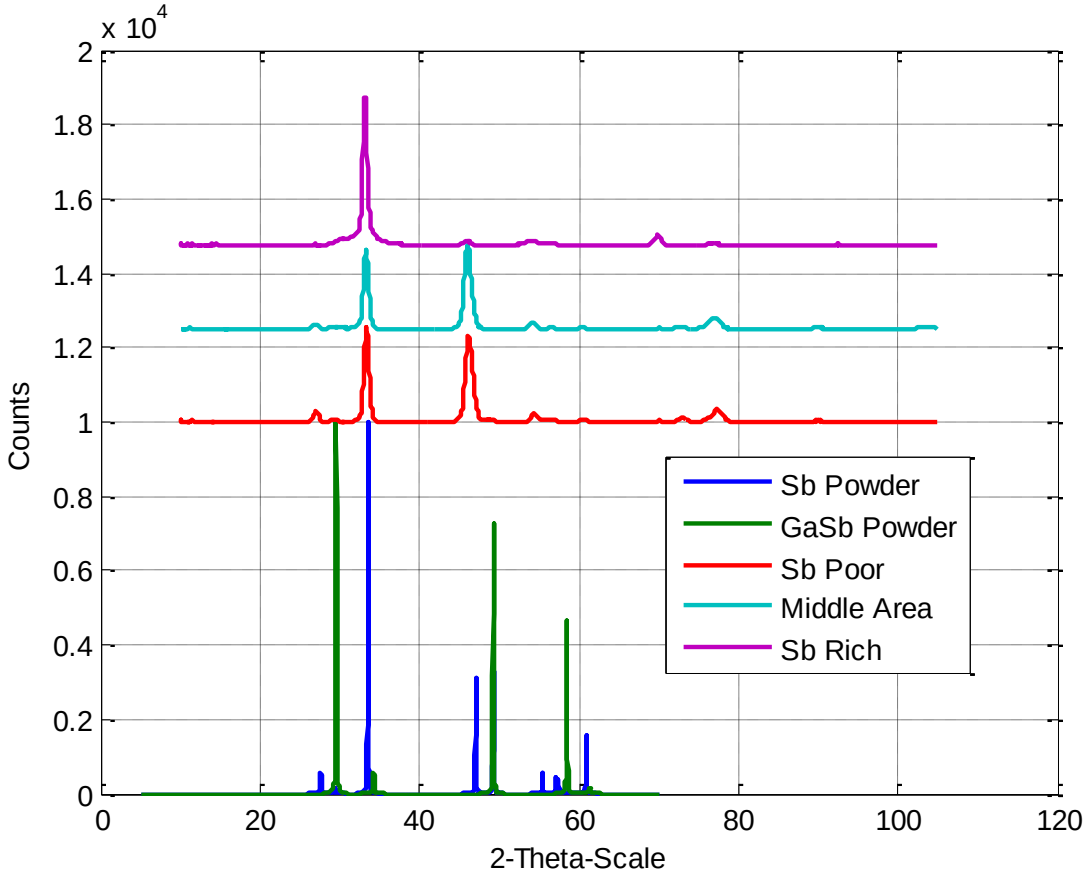

Figure 4.6: X-ray data of GaSb growth attempt 6

Table 4.5: Growth Conditions of GaSb Growth Attempt 7

Base Pressure	Recorded growth Temperature	Heater Power	Argon Flow Rate	Growth Pressure	Sputtering Power
2.1 x 10^{-5} Torr	406 ^{o}C	NA	103 ml/min	10.5 mTorr	80 Watts

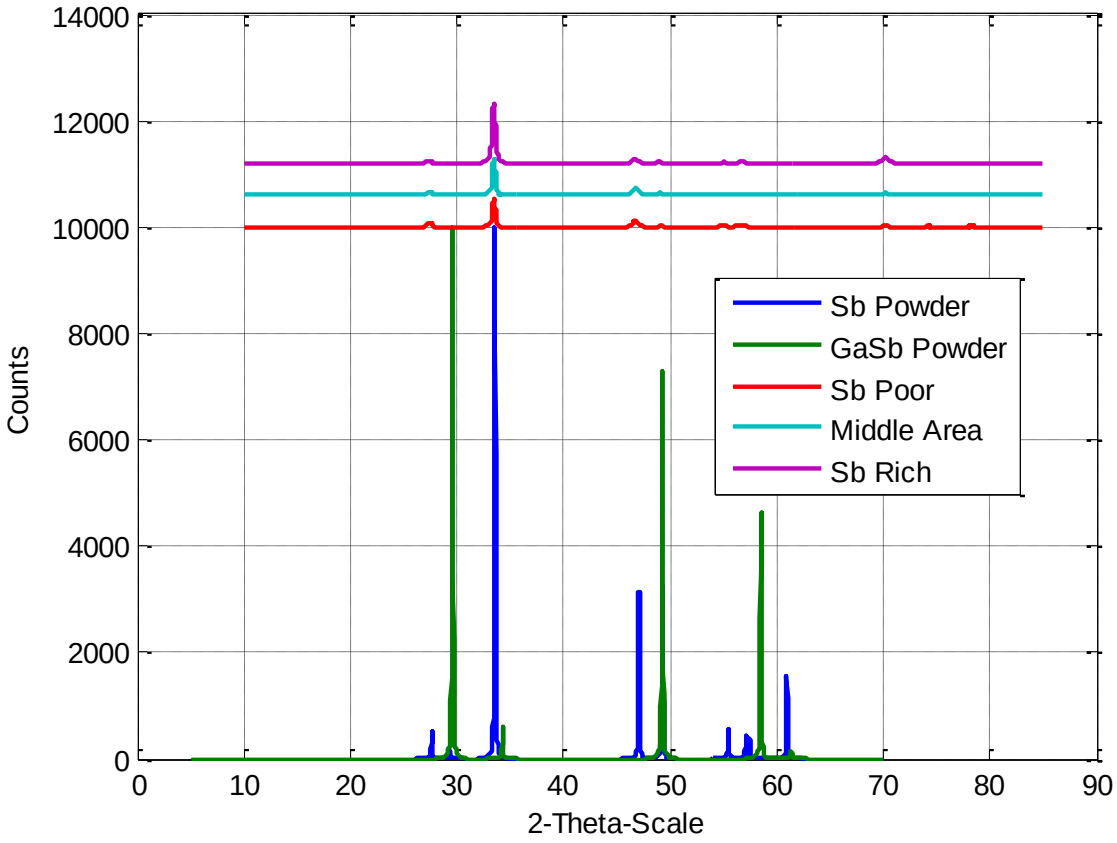

Figure 4.7: X-ray data of GaSb growth attempt 7

Table 4.6: Growth Conditions of GaSb Growth Attempt 8

Base Pressure	Recorded growth Temperature	Heater Power	Argon Flow Rate	Growth Pressure	Sputtering Power
1.5 x 10^{-5} Torr	430 °C	200 Watts	103 ml/min	8.5 mTorr	72 Watts

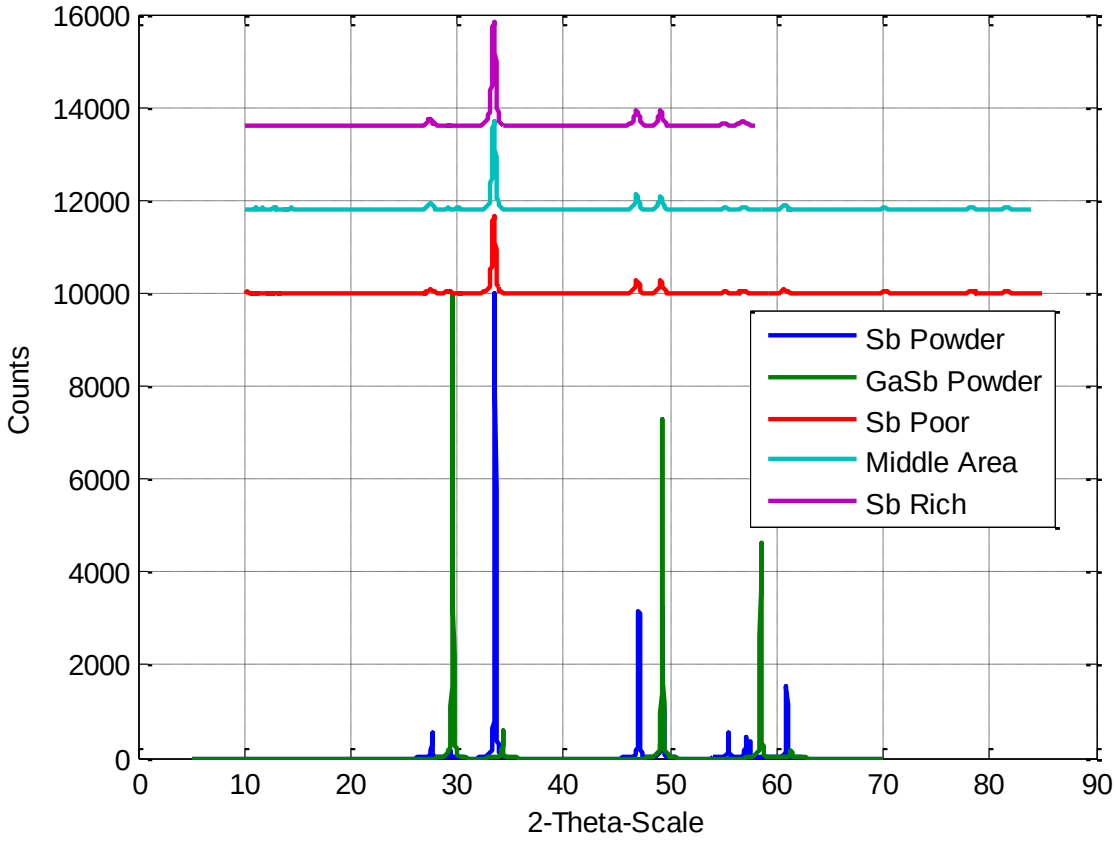

Figure 4.8: X-ray data of GaSb growth attempt 8

Table 4.7:Growth Conditions of GaSb Growth Attempt 9

Base Pressure	Recorded growth Temperature	Heater Power	Argon Flow Rate	Growth Pressure	Sputtering Power
1.5 x 10^{-5} Torr	315 ^{o}C	130 Watts	103 ml/min	8.5 mTorr	72 Watts

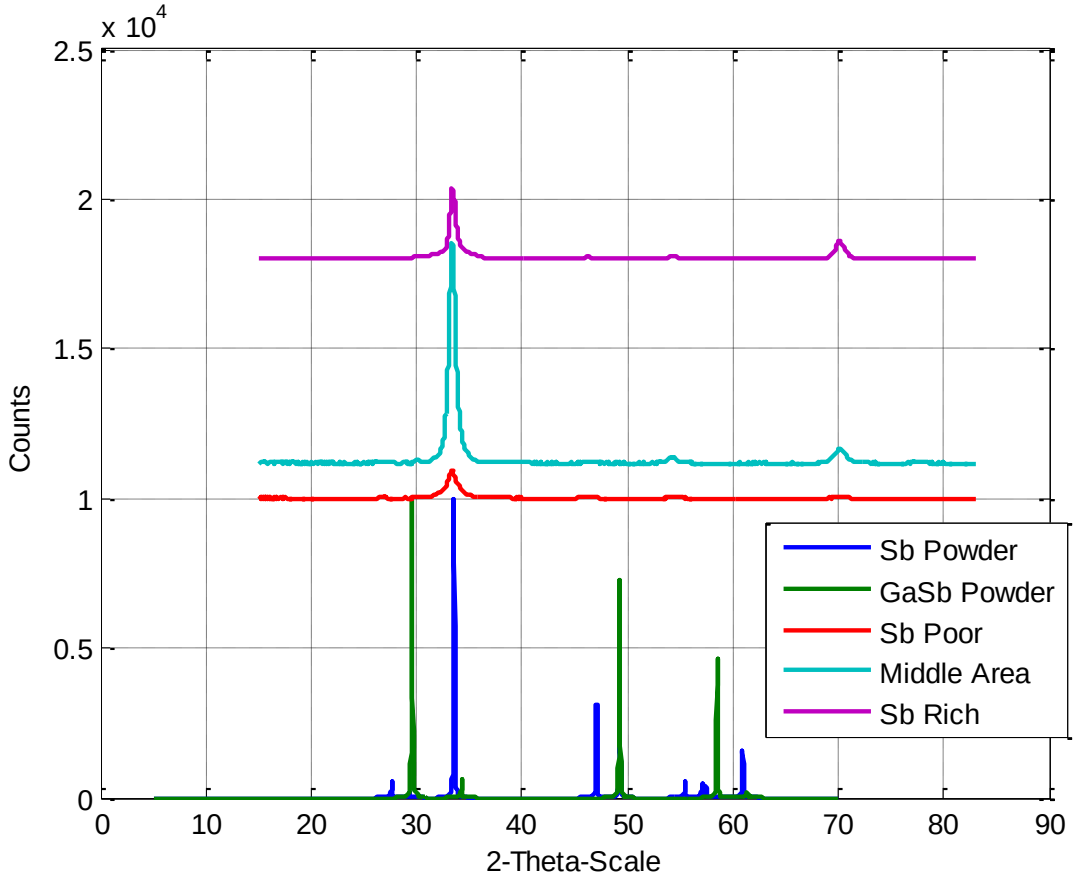

Figure 4.9: X-ray data of GaSb growth attempt 9

Table 4.8: Growth Conditions of GaSb Growth Attempt 10

Base Pressure	Recorded growth Temperature	Heater Power	Argon Flow Rate	Growth Pressure	Sputtering Power
1.7 x 10^{-5} Torr	240 °C	105 Watts	103 ml/min	8.6 mTorr	72 Watts

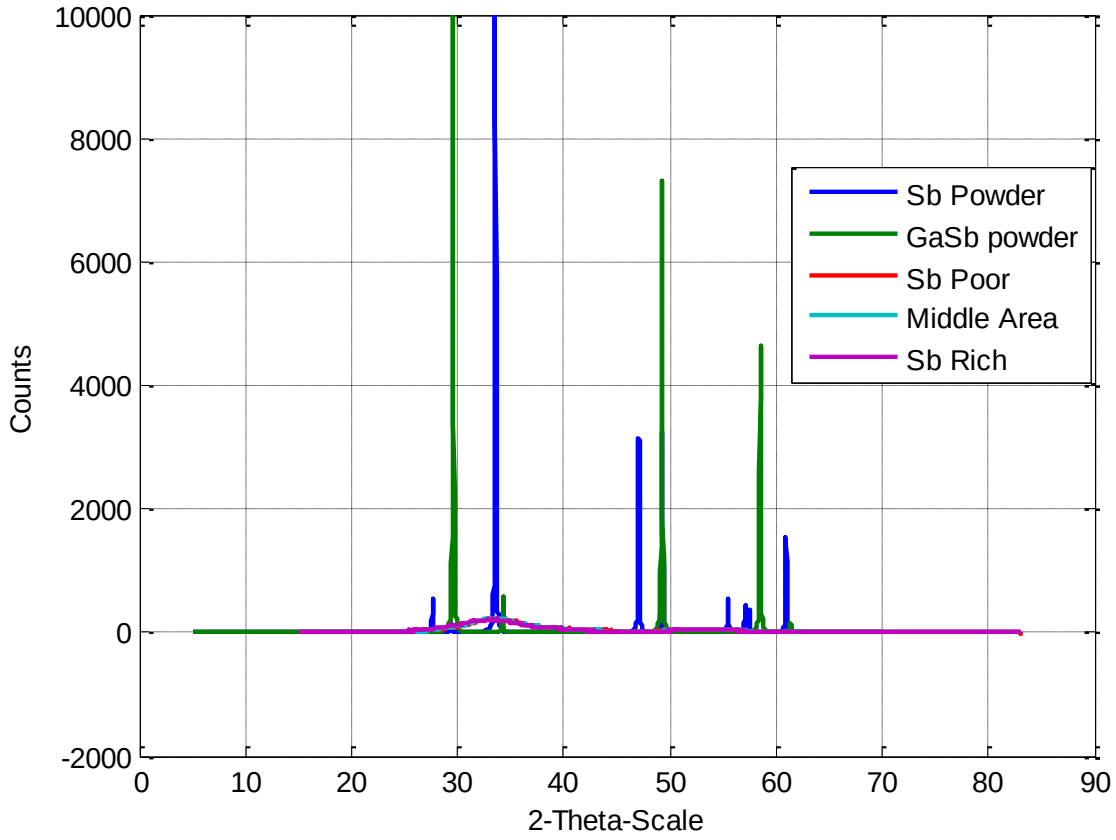

Figure 4.10: X-ray data of GaSb growth attempt 10

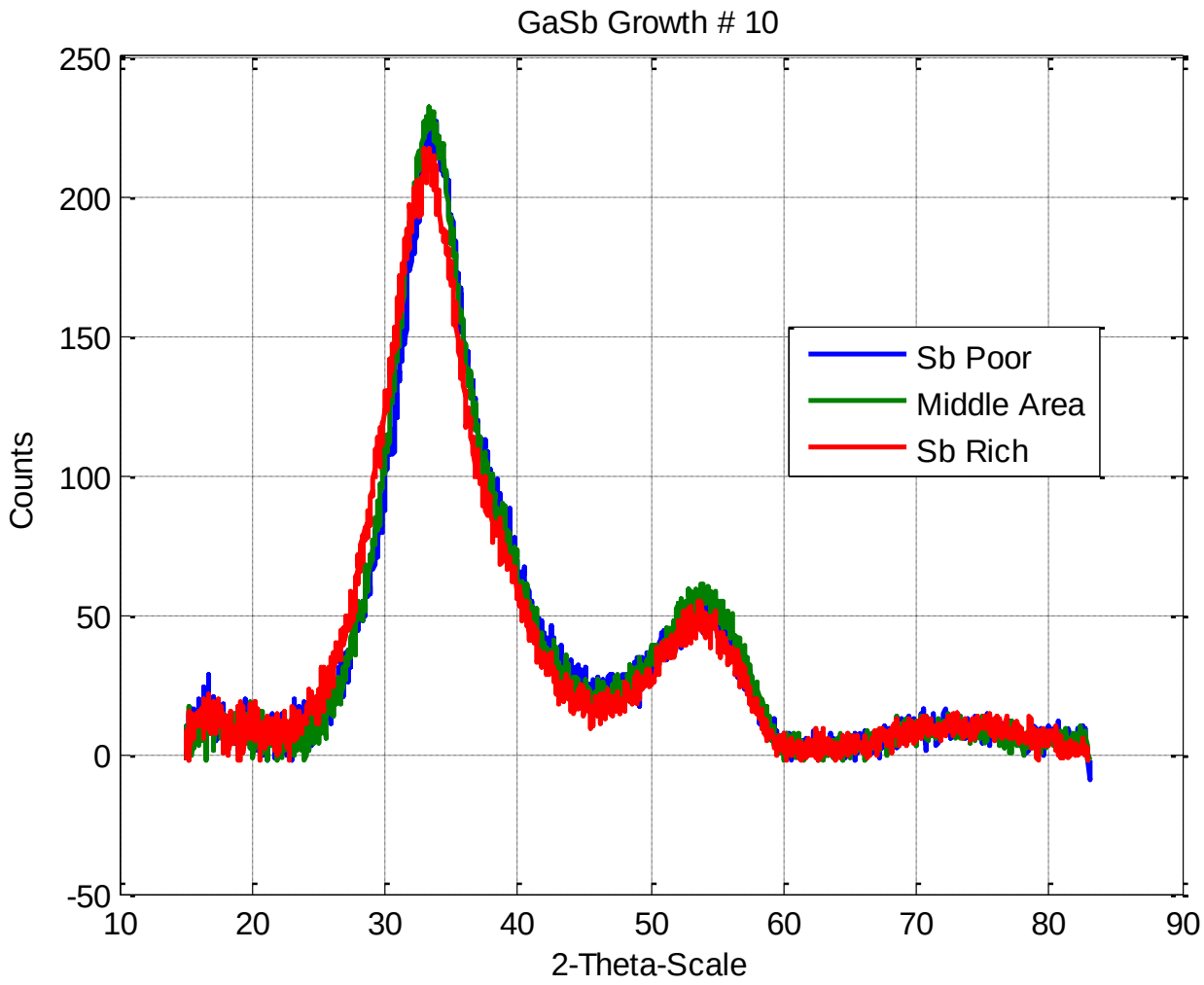

Figure 4.11: Close up of X-ray data of GaSb growth attempt 10

Table 4.9: Growth Conditions of GaSb Growth Attempt 12

Base Pressure	Recorded growth Temperature	Heater Power	Argon Flow Rate	Growth Pressure	Sputtering Power
1.4 x 10^{-5} Torr	418 °C	200 V	103 ml/min	8.5 mTorr	70 Watts

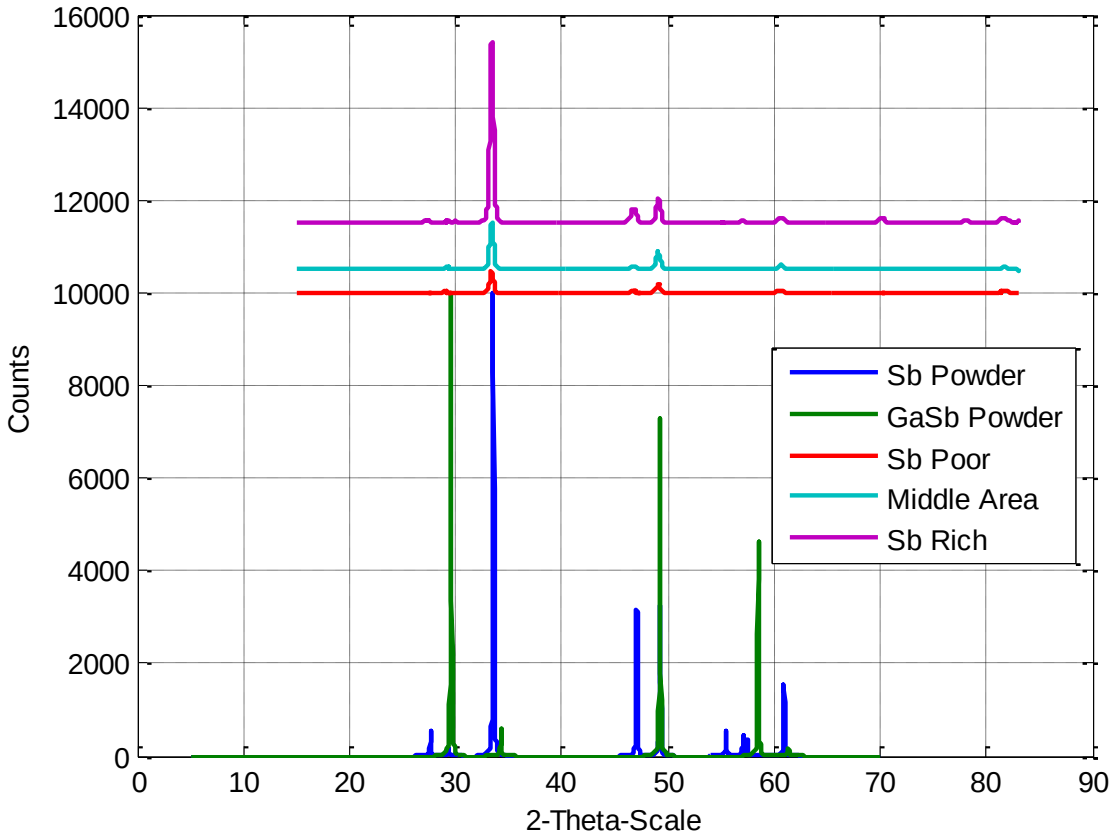

Figure 4.12: X-ray data of GaSb growth attempt 12

Table 4.10: Growth Conditions of GaSb Growth Attempt 13

Base Pressure	Recorded growth Temperature	Heater Power	Argon Flow Rate	Growth Pressure	Sputtering Power
1.4 x 10^{-5} Torr	357 °C	175 Watts	103 ml/min	8.4 mTorr	72 Watts

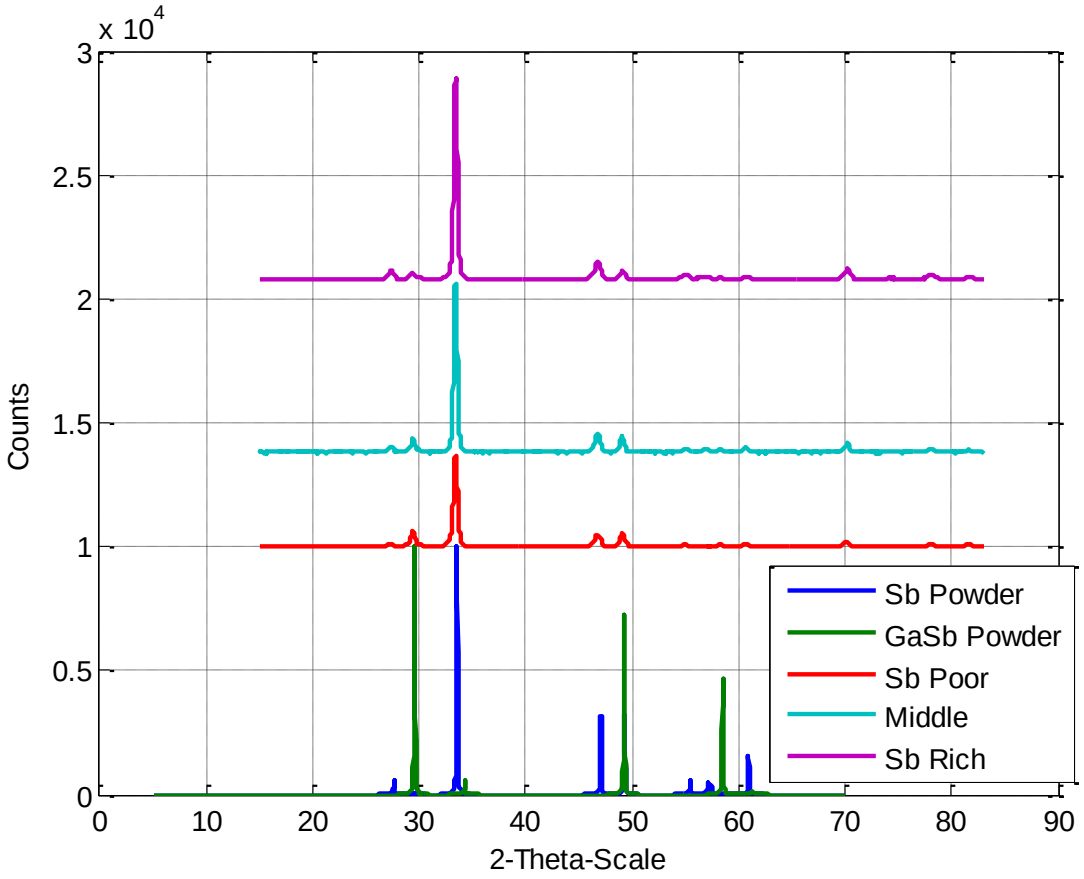

Figure 4.13: X-ray data of GaSb growth attempt 13

Table 4.11: Growth Conditions of GaSb Growth Attempt 14

Base Pressure	Recorded growth Temperature	Heater Power	Argon Flow Rate	Growth Pressure	Sputtering Power
1.5 x 10^{-5} Torr	445 °C	150 Watts	103 ml/min	8.7 mTorr	72 Watts

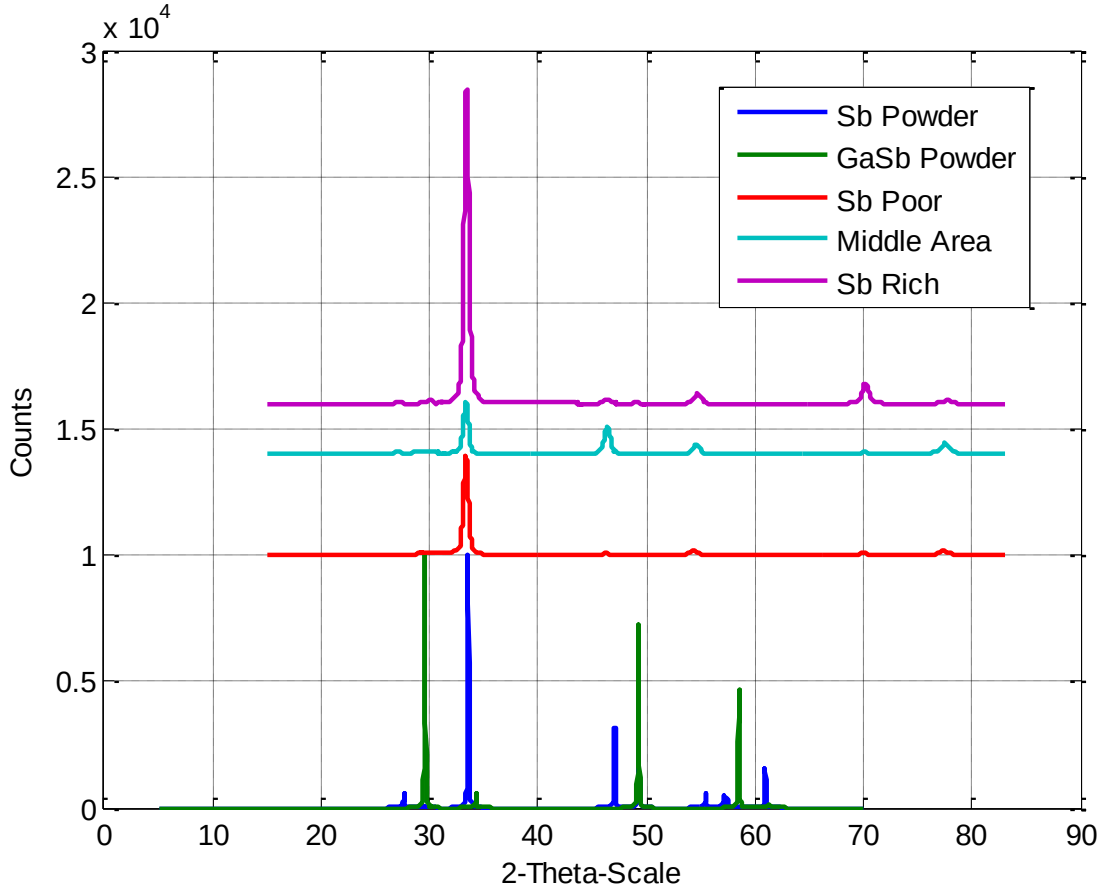

Figure 4.14: X-ray data of GaSb growth attempt 14

Table 4.12: Growth Conditions of GaSb Growth Attempt 15

Base Pressure	Recorded growth Temperature	Heater Power	Argon Flow Rate	Growth Pressure	Sputtering Power
1.3 x 10^{-5} Torr	409 °C	225 Watts	103 ml/min	8.5 mTorr	72 Watts

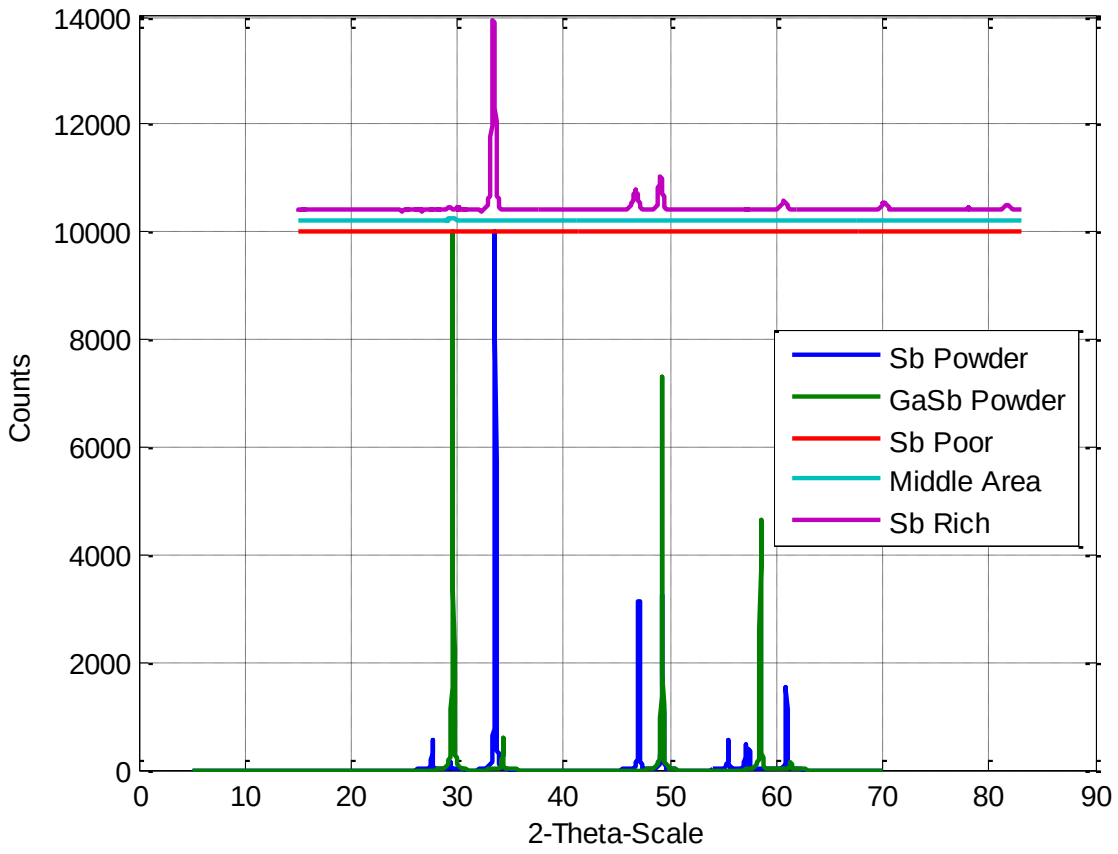

Figure 4.15: X-ray data of GaSb growth attempt 15

Table 4.13: Growth Conditions of GaSb Growth Attempt 17

Base Pressure	Recorded growth Temperature	Heater Power	Argon Flow Rate	Growth Pressure	Sputtering Power
1.8 x 10^{-5} Torr	515 °C	275 Watts	103 ml/min	8.6 mTorr	72 Watts

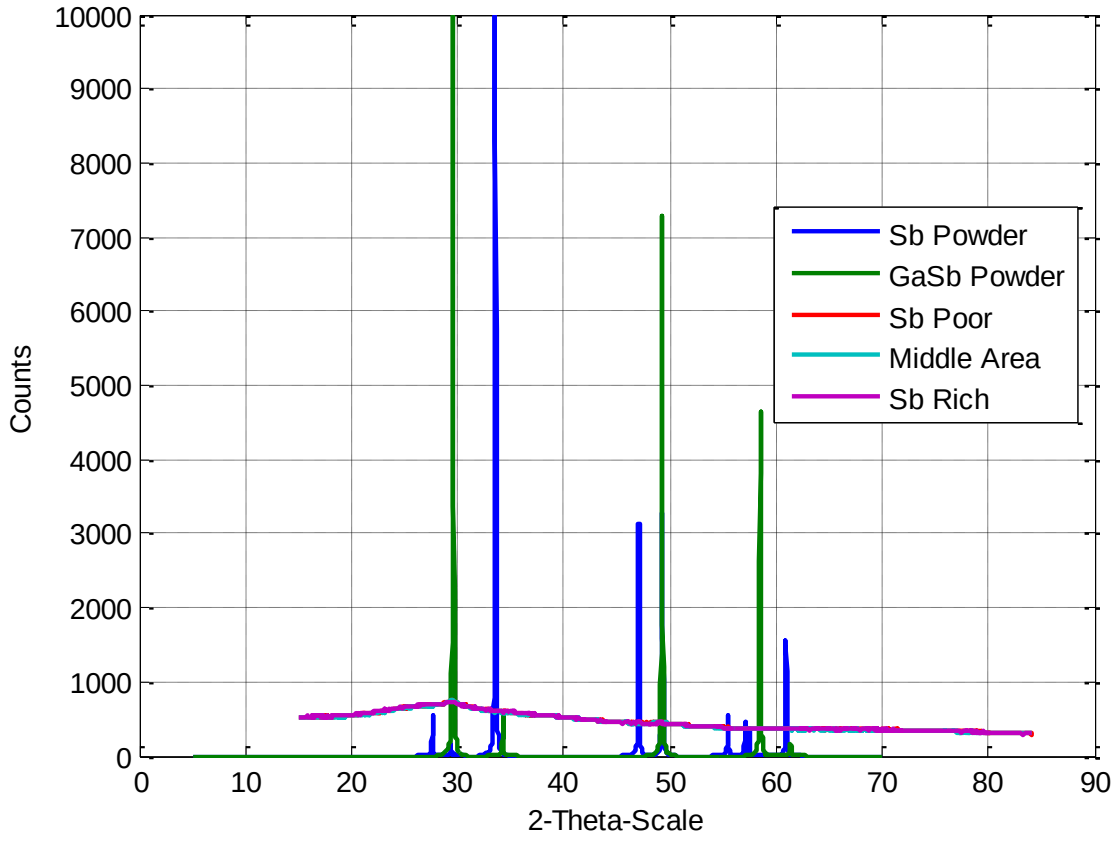

Figure 4.16: X-ray data of GaSb growth attempt 17

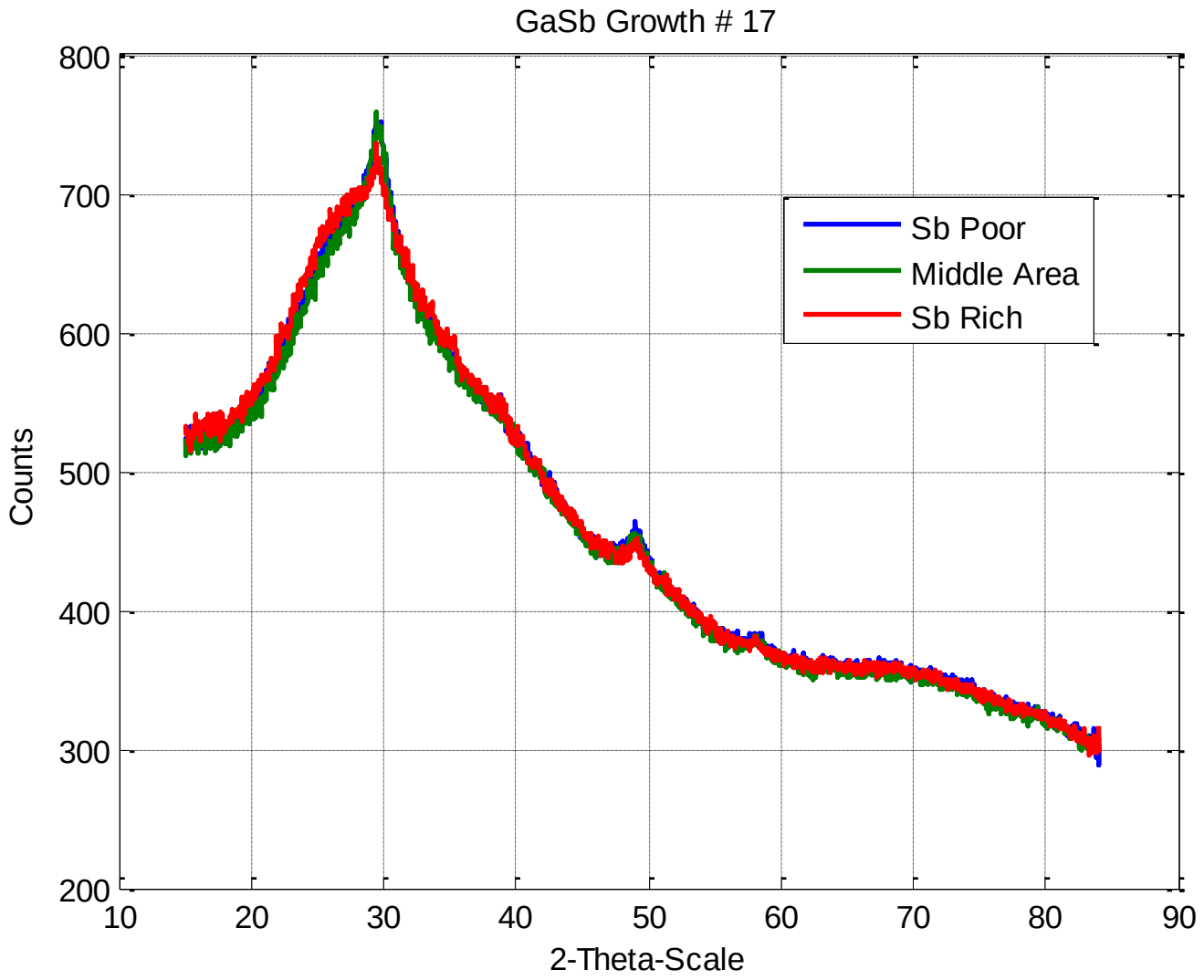

Figure 4.17: Close up of X-ray data of GaSb growth attempt 17

Table 4.14: Growth Conditions of GaSb Growth Attempt 18

Base Pressure	Recorded growth Temperature	Heater Power	Argon Flow Rate	Growth Pressure	Sputtering Power
1.3 x 10^{-5} Torr	483	250 Watts	103 ml/min	8.7 mTorr	72 Watts

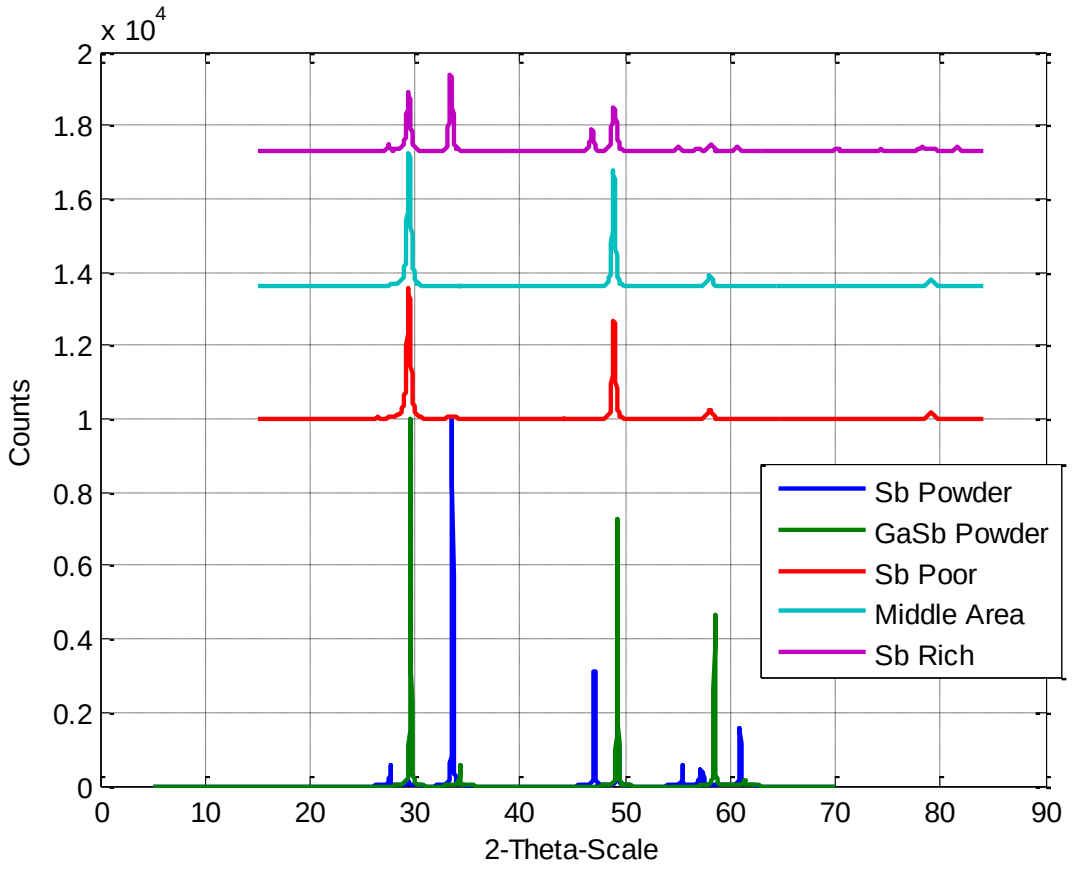

Figure 4.18: X-ray data of GaSb growth attempt 18

4.2 Hall Effect Measurements

Hall Effect measurements were carried on all three different regions of Growth Attempt 18; Sb Poor, Middle Area and Sb Rich. The Hall measurements were conducted at three different temperatures, Room Temperature (300 K), Dry-Ice (195 K) and Liquid Nitrogen (77 K). The experiments were performed in an attempt to measure the carrier activation energy by plotting the log of carrier concentration against reciprocal temperature. The slope of the curve would correspond to the activation energy (E_a), the amount of energy required to excite a free charge carrier into the valence band. In an undoped semiconductor this energy would be equivalent to the band energy gap of the samples.

4.2.1 Hall Effect Measurements Results:

Undoped GaSb is often accompanied with a natural defect where Ga atoms tend to substitute with Sb sites making the material a natural p-type. The Hall Effect results suggest a p-type semiconductor species present as the Ecopia HMS-3000 determines a materials type by the sign of the bulk carrier concentration. Hall Effect Measurements were incapable of producing results in the Sb Poor region at both Dry-Ice and Liquid Nitrogen temperatures. This is thought to be attributed to the presence of the Sb phase. A summary of the Hall measurements are provided in tables (4.15- 4.17). The input current of tables (4.15 and 4.16) were at 100 µA where table 4.17 had an input current of 10 µA.

Table 4.15: Sb Poor Hall Effect Measurements conducted at 100 µm

Temperature (K)	Bulk Concentration (cm^{-3})	Mobility (cm^2/Vs)	Resistivity Ωcm	Hall Coefficient (cm^3/C)
Room Temperature (300K)	1.456×10^{20}	2.542×10^{-1}	1.687×10^{-1}	1.909×10^{-1}
Dry-Ice (195 K)	5.005×10^{18}	6.175×10^{0}	2.020×10^{-1}	2.514×10^{0}
Liquid Nitrogen (77 K)	7.289×10^{17}	4.302×10^{1}	1.99×10^{-1}	1.672×10^{0}

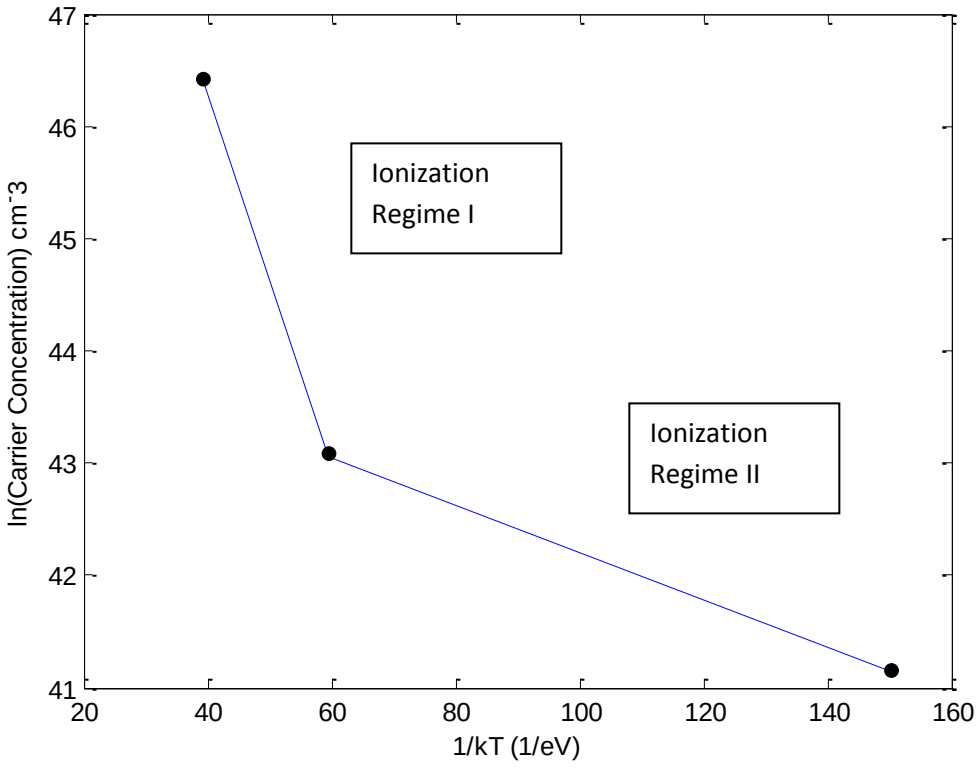

Figure 4.19: Carrier concentration vs. 1/kT (1/eV) of Hall measurement data for Sb Poor region

Table 4.16: Middle Area Hall Effect Measurements conducted at 100 µm

Temperature (K)	Bulk Concentration (cm^{-3})	Mobility (cm^2/Vs)	Resistivity Ωcm	Hall Coefficient (cm^3/C)
Room Temperature (300K)	7.545×10^{19}	1.645×10^{0}	5.030×10^{-2}	1.641×10^{-2}
Dry-Ice (195 K)	9.668×10^{18}	3.720×10^{1}	1.736×10^{-2}	1.425×10^{0}
Liquid Nitrogen (77 K)	2.916×10^{17}	2.628×10^{2}	8.147×10^{-2}	1.715×10^{0}

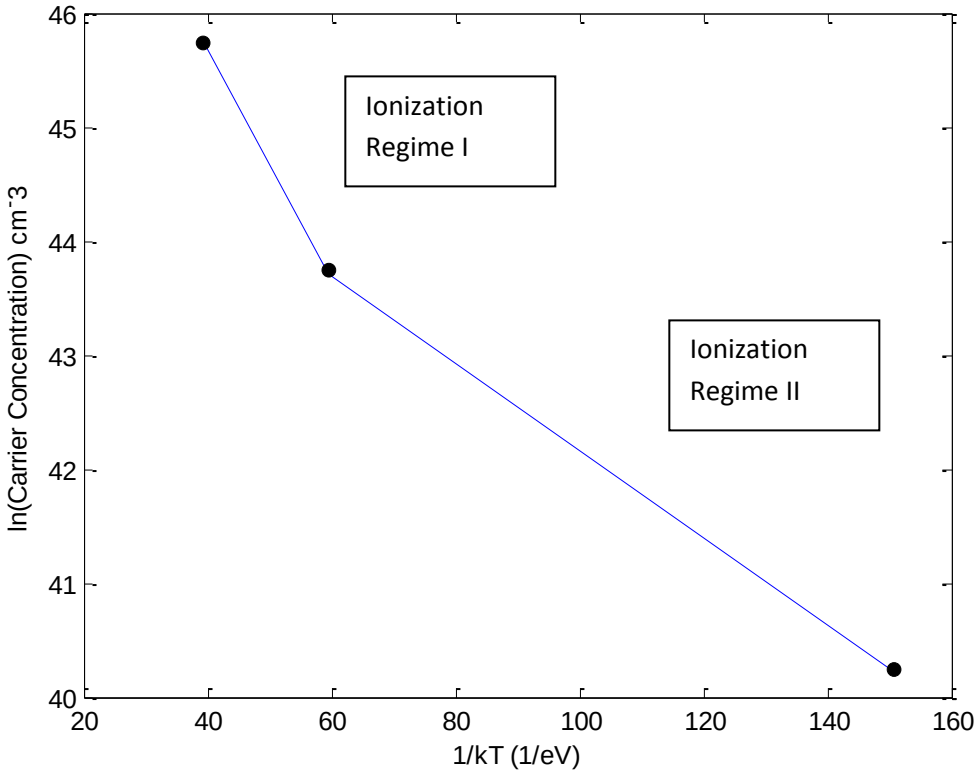

Figure 4.2027: Carrier concentration vs. 1/kT (1/eV) of Hall measurement data for Middle Area region

Table 4.17: Sb Rish Hall Effect Measurements conducted at 100 µm

Temperature (K)	Bulk Concentration (cm^{-3})	Mobility (cm^2/Vs)	Resistivity Ωcm	Hall Coefficient (cm^3/C)
Room Temperature (300K)	1.114×10^{19}	4.699×10^{-2}	1.193×10^{1}	1017×10^{1}
Dry-Ice (195 K)	NA	NA	NA	NA
Liquid Nitrogen (77 K)	NA	NA	NA	NA

Extracting data from the Hall Effect measurements resulted in figures 4.19 and 4.20. Ionization Regime I corresponds to the ionization region between room temperature and Dry-Ice temperature where Ionization Regime II corresponds to the ionization region between Dry-Ice region and liquid Nitrogen region. There activation energy can be found by measuring the slope of each region where it corresponds to the amount of energy needed to promote a charge carrier from the carrier level to the valence band at their corresponding temperatures. The points on the curves seen in figures 4.19 and 4.20 represent the carrier concentration at their respective temperature. Since only three temperatures were used, there was not enough data points to accurately determine the shape and slope of the curve. Therefore the calculated activation energy is only an approximation. The following table summarizes the activation energy of each region in the GaSb film:

Table 4.18: Summary of Activation Energies of GaSb Growth Attempt 18

Regimes	E_a for Sb Poor	E_a for Middle Area
Ionization Regime I	0.1672 eV	0.1017 eV
Ionization Regime II	0.058 eV	0.061 eV

it can be seen that the activation energies E_a are substantially lower than the band gap energy of GaSb; 0.72 eV. These low activation energies may be attributed to many factors such as defects within the film that may occurred during growth. It is thought that due to the low activation within the film that may have occurred during growth. It is thought that due to the low activation energy the carrier concentrations are high and therefor a minority carrier life time measurement experiment was unsuccessful.

In previous work [41] Ga vacancies (V_{Ga}) were calculated to have various transition levels in the band gap. A (0/1-) level exists above the valance band maximum at about 0.13 eV. This value is in par with the measured Activation energies in the Ionization Regime I indicating the possibility of the existence Ga anti-sites and vacancies throughout the sample.

4.3 Scanning Electron Microscopy (SEM)

Selected samples were further characterized under the electron microscopy to gain an insight into the grain size and microstructure. Growth attempts 5 and 18 showed apparent GaSb X-ray peaks and for that reason they were selected to be examined under the electron microscope. A cross sectional view was taken for both growth attempts in order to measure their thicknesses. Before noting that the metal rod was creating a hot spot that caused the film to have voids, Growth Attempt 8 was also examined under the SEM.

4.3.1 SEM Results

The figures below show SEM images of the selected samples; 5, 8 and 18. The X-ray data of the growth attempts are seen in figures 4.5, 4.8 and 4.18 which shows a difference in composition of the film species, GaSb and Sb respectively. A distinction is made between the grain structures of all three films. In the case of Growth Attempt 5, the sizes of the grains were seen to be about 400 nm as seen in figure 4.21. Clusters of grains were apparent which may be

due to the non-uniform heat distribution during the growth process. A Cross-sectional view of the sample shows a non-uniform thickness ranging between 1.7 to 2.3 μm as seen in figure 4.23.

GaSb X-rays peaks were not present in Growth Attempt 8 concluding that Sb was the dominant composition throughout the film. Surface SEM images show a smaller grain, about 300 nm as seen in figure 4.24, growth that's is attributed to the different species in comparison to the Growth Attempt 5. A non-uniform thinner sample was produced, 0.441 – 0.6 μm as seen in figure 4.26, during the growth conditions of Growth Attempt 8. This is attributed to the presence of the hot spot region the lower sticking coefficient of Sb at higher temperatures. The conditions of Growth Attempt 18 resulted in apparent GaSb throughout the film. A smaller grain size was apparent, about 150 nm as seen in figure 4.27, when comparing the grain size to Growth Attempt 5. A cross sectional view of Growth Attempt 18 resulted in a near-uniform sample thickness of about 0.45 μm as seen in figure 4.29. The conditions of Growth Attempt 18 resulted in a thinner sample when grown at Growth Attempt 5 conditions. This is attributed to hotter substrate and uniformity heat distribution. As the substrate temperature increased, the Sb seemed less likely to stick on to the substrate slowing down the growth rate of the film. As a result of the slower growth rate, a thinner sample was produced along with a smaller grain size.

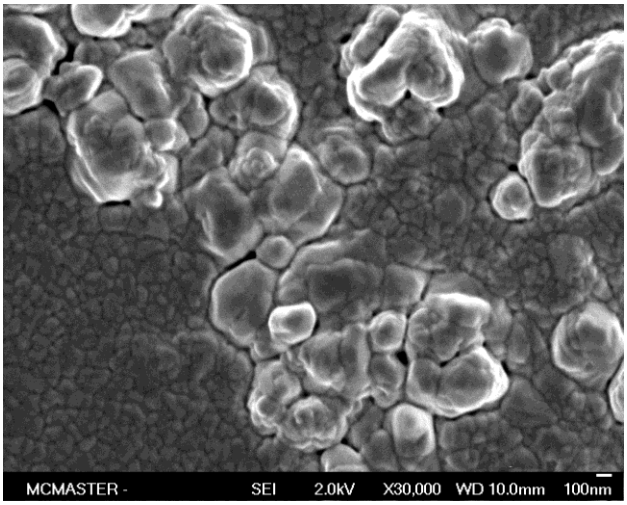

Figure 4.21: SEM Surface view of Growth Attempt 5

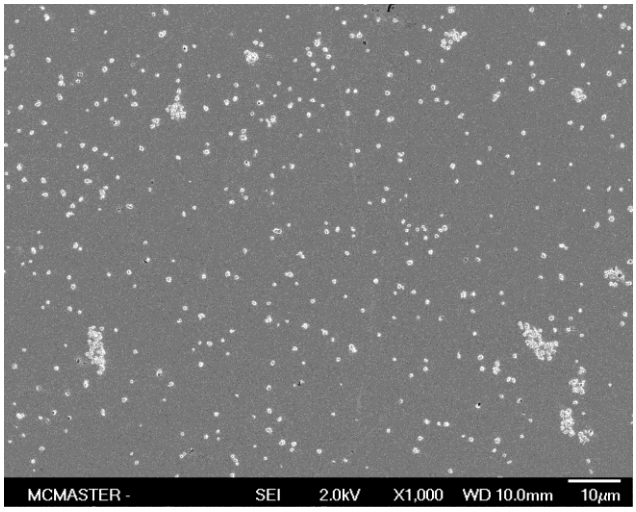

Figure 4.22: SEM Vew of grain size of Growth Attempt 5

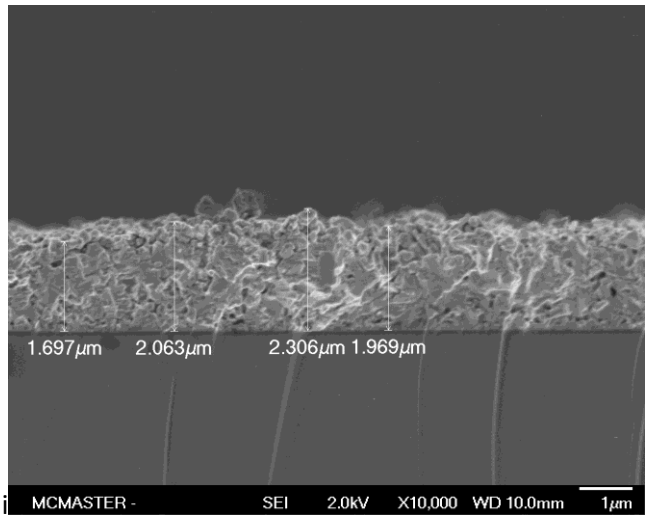

Figure 4.23: SEM Cross sectional view of Growth Attempt 5 showing film thickness

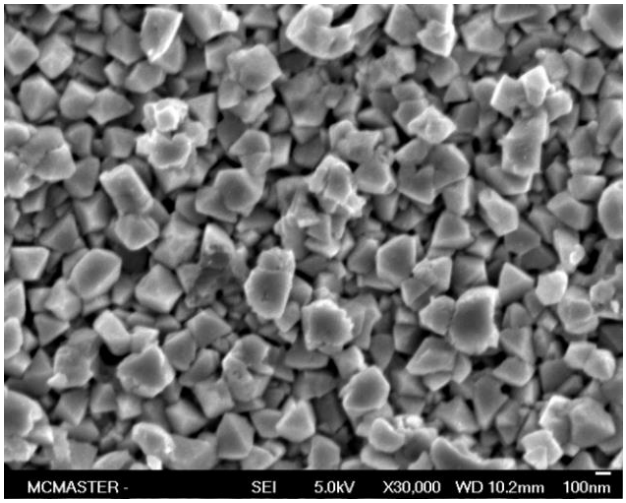

Figure 4.24: SEM View of grain size of Growth Attempt 8

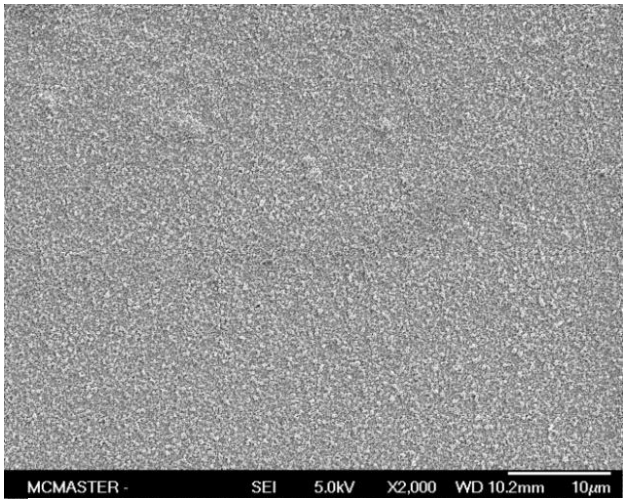

Figure 4.25: SEM Surface view of Growth Attempt 8

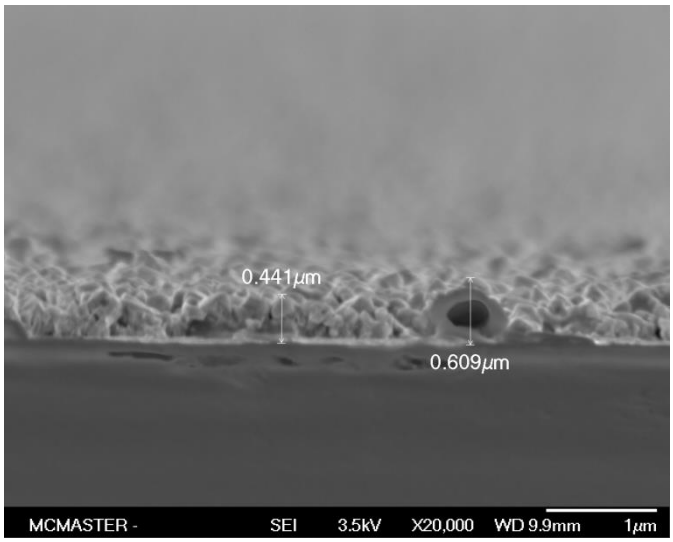

Figure 4.26: SEM Cross sectional view of Growth Attempt 8 showing film thickness

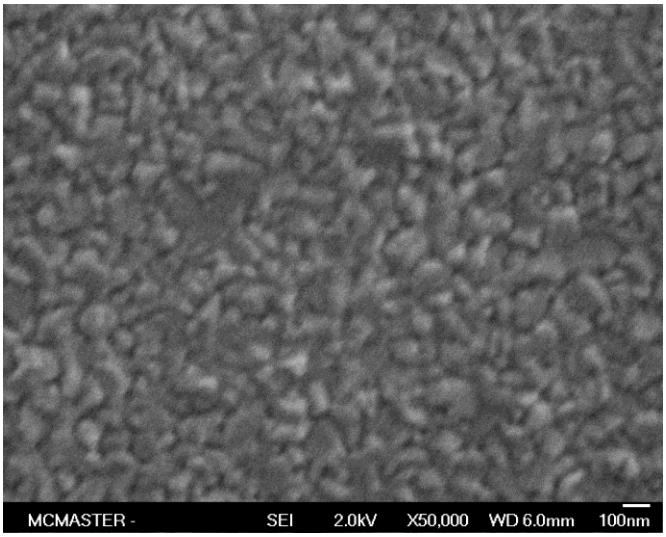

Figure 4.27: SEM View of grain size of Growth Attempt 18

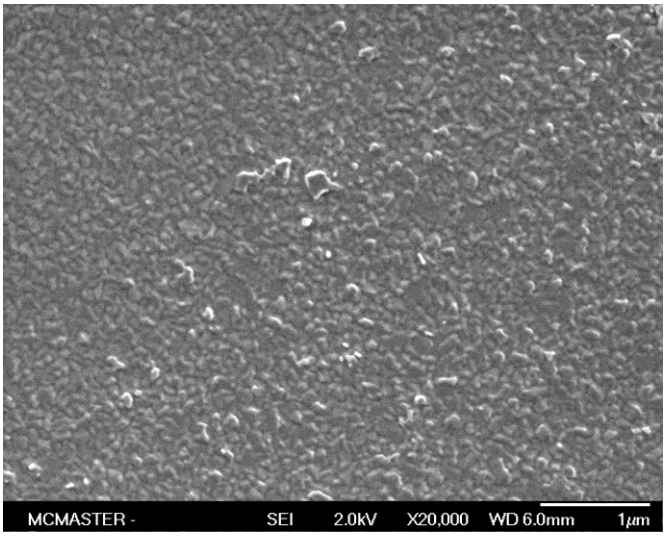

Figure 4.2828: SEM Surface view of Growth Attempt 18

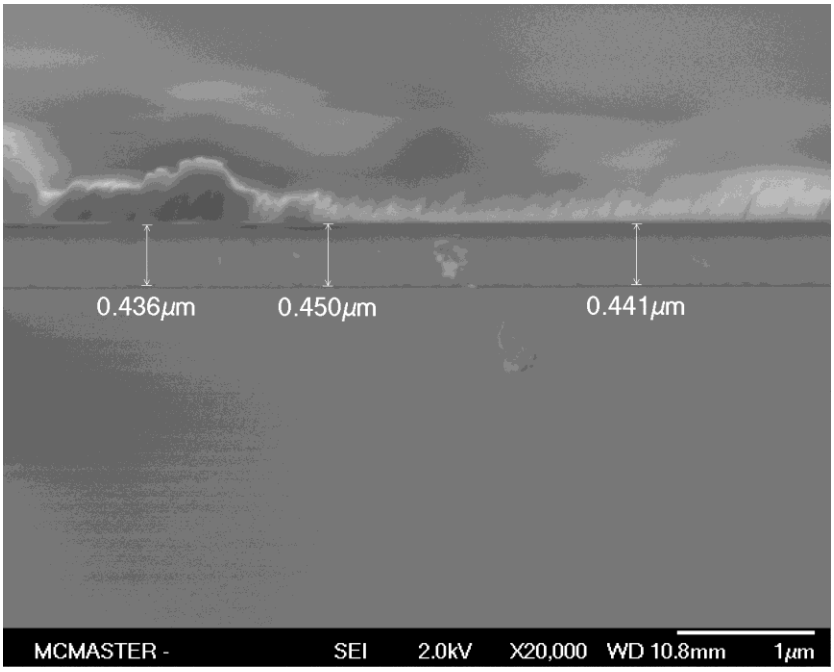

Figure 4.29: SEM Cross sectional view of Growth Attempt 18 showing film thickness

4.4 Fourier Transform Infrared Spectroscopy (FTIR)

FTIR was used as a technique to confirm the refractive index of the grown films alongside to predict the thickness of the film. The Middle Area of Growth Attempts 5 and 18 were used to implement this technique due to its apparent GaSb X-ray peaks. The figures following figures show the percent of transmitted light as a function of wavelength.

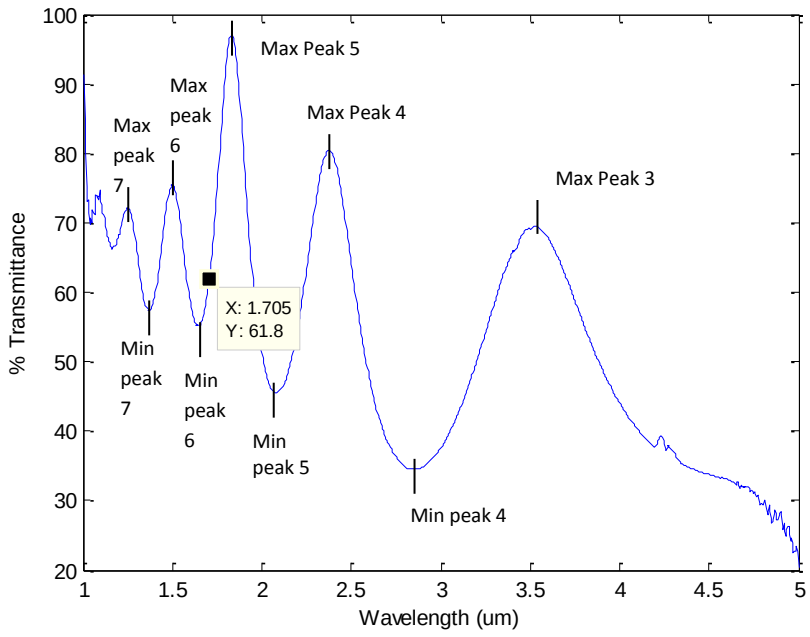

Figure 4.30: % Transmittance vs. Wavelength of Growth Attempt 5 Middle Area indicating the percentage of light transmitted at the band gap of GaSb

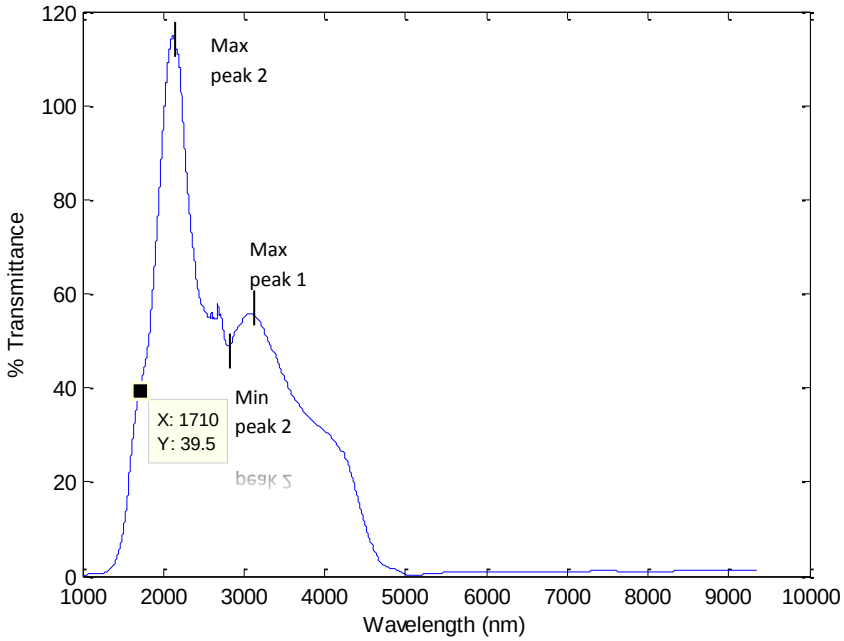

Figure 4.31: % Transmittance vs. Wavelength of Growth Attempt 18 Middle Area indicating the percentage of light transmitted at the band gap of GaSb

As seen in both figures 4.27 and 4.28 a transmission vs. wavelength was produced as the infrared laser is incident on to the surface of the samples. An interference pattern is generated as light transmitted from the film interacts constructively and destructively. Using the constructive and destructive interference equations mentioned in chapter 2 for maximum and minimum transmission is seen below:

$$\text{Maximum Transmission: } 2d = n\,\frac{\lambda}{n_{refract}}$$

$$\text{Minimum Transmission: } 2d = \frac{(2n-1)}{2}\,\frac{\lambda}{n_{refract}}$$

where d corresponds to the thickness of the grown film, λ corresponds to the wavelength of light incident onto the film, $n_{refract}$ corresponds to the refractive index of the film and n is a positive integer where n = 1,2,3,…

A sample thickness was attempted to be calculated with a refractive index of 3.8 where n, the integer multiples, corresponded to the peak numbers labeled in figures 4.30 and 4.31. Tables 4.19 and 4.20 summarize thickness measurements attempted by extracting the data from the FTIR curves.

Table 4.19: Summary of theoretical thicknesses of Growth Attempt 5 extracted from FTIR

n	λ (μm)	Maximum Transmission thickness (μm)	λ (μm)	Minimum Transmission thickness (μm)
3	3.54	1.39	NA	NA
4	2.4	1.26	2.85	1.31
5	1.84	1.21	2.08	1.23
6	1.48	1.17	1.64	1.18
7	1.265	1.16	1.37	1.17

Table 4.20: Summary of theoretical thicknesses of Growth Attempt 18 extracted from FTIR

n	λ (μm)	Maximum Transmission thickness (μm)	λ (μm)	Minimum Transmission thickness (μm)
1	3.13	0.41	NA	NA
2	2.15	0.56	2.81	0.55

When attempting to calculate the thickness of the samples it was expected that the values calculated would stay constant while changing the values of n. in the case of Growth Attempt 5, it was unclear how the film reacted to light beyond 5 µm. For that, different values of n were assumed until a constant thickness values were obtained. The thicknesses obtained were not constant as n changes however, using the values of n recorded in table 4.18 yielded to similar thicknesses for both maximum and minimum transmission.

As seen in figure 4.31, Growth Attempt 18 is nearly absorbent of light at a wavelength beyond 5 µm and one minimum transmission peaks is apparent. The peaks labeled on the graph were used as values of n. A theoretical thickness of about 0.55 µm was calculated for a minimum transmission at a value of n = 2. A peak corresponding to an n value of 1 is not distinct in figure 4.31 for that n = 1 was not used in attempt to predict a theoretical thickness. A maximum transmission peak is apparent at a wavelength of 3.13 µm resulting in a predicted thickness of 0.41 µm. the second maximum transmission peak is has a wavelength value close to the band edge resulting in a predicted thickness of 0.56 µm.

4.5 Alpha Stepper

An alpha stepper was used as a third method of measuring a sample thickness. The Sb-poor region of Growth Attempt 18 was used to conduct this experiment due to an apparent difference in thickness between the film and the exposed glass from the edges of the substrate. The exposed glass was located at the edges of the substrate due to the locking mechanism covering small portions of the substrate at the both ends of the substrate. As seen in figure 4.32. a thickness value of 0.6 µm was measured.

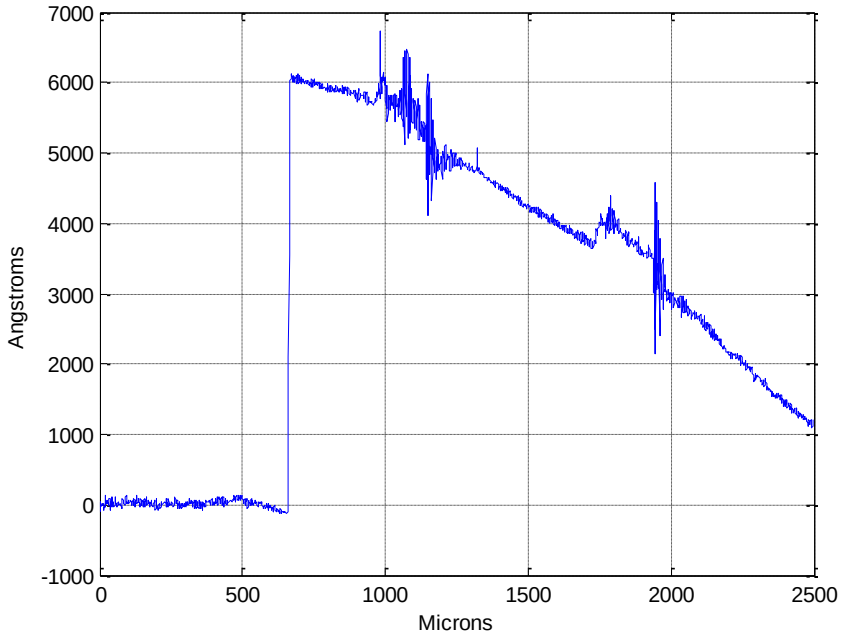

Figure 4.32: Alpha Step thickness measurements of the Sb-poor region of Sample 18 were the thickness of the sample corresponds to the step

Chapter 5: Conclusions and Future Work

5.1 Conclusions

The growth via sputtering of GaSb films was conducted from a Gab split-target onto a glass substrate. The GaSb target was fabricated and molded using pure elements. Electrical and optical characterization techniques have been investigated of each film.

Molding a GaSb split target was unsuccessful when placing both Ga and Sb in an open crucible inside an argon atmosphere tube furnace. This resulted in the excess Sb sinking to the bottom of the mold. Placing both the Ga and Sb elements in a vacuumed sealed ampule where the ampule was placed inside a box furnace was successful in forming the GaSb compound. GaSb was then molded in an argon atmosphere into the desired semicircular shape.

GaSb films were successfully grown when the substrate was suspended with clips at an input heater power of 280 watts. Placing the substrate in direct contact with a metal heater plate resulted in unsuccessful GaSb film growth. An amorphous Sb film was produced at low substrate temperature. A substrate failure then occurred as a result of a higher substrate temperature. Altering the design of the metal heater plate and placing the substrate further from the sputtering target produced a successful growth of a GaSb film at heater power of 250 watts.

Hall Effect measurements conducted on the film grown with a heater power of 280 watts were unsuccessful. This was a result of an apparent virtual short circuit when probing the sample with an ohm meter. Conducting the experiment on the film grown at a heater power of 250 watts was successful and resulted in p-type semiconductor with high carrier concentrations; 1.456×10^{20} cm^{-3}, 7.545×10^{19} cm^{-3} and 9.8×10^{20} cm^{-3} for Sb Poor, Middle Area and Sb Rich

regions of the substrate respectively. Hall Effect measurements conducted on the film grown with a heater power of 250 watts at Dry-Ice temperature and liquid nitrogen temperature was only successful in Sb Poor and the Middle Area of the film. This resulted in carrier concentrations of $5.005\ x10^{18}\ cm^{-3}$ and $7.289\ x10^{17}\ cm^{-3}$ for Dry-Ice and liquid nitrogen temperatures respectively in the Sb Poor Area. These results went on to exhibit low activation energies of 0.1672 eV and 0.058 eV. These low activation energies indicate a poor quality GaSb film with major defects in the Sb Poor region. The activation energies of the Middle Area were also found to be low at 0.1017 eV and 0.061 eV. The measured activation energies conclude the presence of defects throughout different regions of the film where we identified them as possible anti-sites.

Mobility values for the film grown at a heater power of 250 watts were found to be low and unsuitable for the design of a solar cell. Comparing the measured mobility values, $4.302\ x10^{1}\ cm^2/Vs$ and $2.628x10^{2}\ cm^2/Vs$ for the Sb Poor and Middle Area respectively at 77 ^{o}K, with the literature mobility value of $2.7\ x10^{2}\ cm^2/Vs$ at 77 ^{o}K is attributed with to the presence of a high carrier concentration.

FTIR concluded a theoretical thickness with a 14% error, when comparing to SEM, for the film grown at a heater power of 280 watts demonstrating the light interfering constructively and destructively. As for the film grown at a heater power of 250 watts, FTIR concluded the sample to be absorbent beyond the 5 μm wavelength and to have luminescent properties between the 2μm and the 2.5 μm where the band gap of GaSb is about 1.72 μm. A theoretical thickness error for minimum transmission was about 18%. A maximum transmission thickness error of about 10% was calculated for the apparent peak corresponding to a wavelength of 3.13

μm. The maximum transmission peak corresponding to wavelength of 2.15 μm is concluded to be significantly influenced by the band edge.

An Alpha Step measurement concluded a film thickness of 6 μm. the measurements were conducted on the film grown at a heater power of 280 watts at the Sb-poor region. When comparing the measured thickness to the theoretical thickness calculated using FTIR a 4 % standard error is observed. Possible sources of error may be the result of the difficulty of performing a thickness measurement with the Alpha Step in exact location where the FTIR data was collected.

SEM concluded the presence of GaSb crystal growth for both films grown at heater powers of 250 and 280 watts. SEM also concluded a non-uniform thickness of film grown at a heater power of 250 watts and a grain size of around 300 nm. Analyzing the surface of the film also showed clusters of GaSb grains forming throughout the film along with the presence of a sub-grain layer.

5.2 Future Work

The growth of GaSb films from a split-target was demonstrated in this work. Although Hall Effect measurements were successful in finding the carrier concentrations of the film, carrier lifetime measurements were unsuccessful due to a high carrier concentration having along with the low activation energy. The low activation energy is attributed to defects during the growth process. However, we are not sure of the exact assignment of these defects although anti-sites are a distinct possibility. Future work should be focused on altering the growth parameters to achieve a lower carrier concentration, higher mobility value and an activation energy value as close to the value of the band gap.

REFERENCES:

[1] McLamb, E. (2011, 09 18). *The Ecological Impact of the Industrial Revolution*. Retrieved from http://www.ecology.com/2011/09/18/ecological-impact-industrial-revolution/

[2] Vidal, J. (2014, 06 23). *UK and Germany break Solar Power Records*. Retrieved from http://www.theguardian.com/environment/2014/jun/23/uk-and-germany-break-solar-power-records

[3] Wael Mahdi, B. (2014, 05 20). Retrieved from Saudi Oil Company Seeks More Solar Power : http://www.renewableenergyworld.com/rea/news/article/2014/05/saudi-arabian-oil-company-seeks-more-solar-power

[4] The Ntional Staff. (2014, 06 04). Retrieved from UAE ranks third in the world for total solar power capacity and investment, says report: http://www.thenational.ae/uae/technology/uae-ranks-third-in-the-world-for-total-solar-power-capacity-and-investment-says-report

[5] Brownson, J. R. (2013). Solar Energy Conversion Systems. Academic Press .

[6] Reece, W. (n.d.). *The History Of Solar Power*. Retrieved from https://www.experience.com/alumnus/article?channel_id=energy_utilities&source_page=additional_articles&article_id=article_1130427780670

[7] A. Polman, H. A. (2012). Photonic design principles for ultrahigh-efficiency photovoltaics. *Nature Materials*.

[8] Dimroth, D. F. (2013, 09 23). *World Record Solar Cell with 44.7% Efficiency*. Retrieved from http://www.ise.fraunhofer.de/en/press-and-media/press-releases/presseinformationen-2013/world-record-solar-cell-with-44.7-efficiency

[9] l. M. Fraas, G. R. (1989). GaSb booster cells for over 30% efficient.solar-ceU stacks. *J.Appl.Phys.*, 3866-3870.

[10] Fraas, L., Avery, J., Martin, J., Sundaram, V., Girard, G., Dinh, V., et al. (1990). Over 35-Percent Efficient GaAs /GaSb Tandem Solar Cells. *Electron Devices, IEEE*, 443-449.

[11] Ben Streetman, S. K. (2006). *Solid State Electronic Devices, 6th Ed.* New Jersey: Pearson Education Inc.

[12] Rachel Casidy, R. F. (n.d.). *Bonds, Bands, and Doping:*. Retrieved from http://www.chemistry.wustl.edu/~edudev/LabTutorials/PeriodicProperties/MetalBonding/MetalBonding.html

[13]: Kitai, A.H. (2011*). Principles of Solar Cells, LEDs and Diodes: The role of the PN junction*, 1st Ed, Wiley-Blackwell.

[14]: Science, P. S. (n.d.). *Semiconductors*. Retrieved from https://online.science.psu.edu/phys010_archive_suwd/node/8363

[15]: P. S. Dutta, H. L. (1997). The physics and technology of gallium antimonide: An emerging optoelectronic. *Journal of Applied Physics*, 5821-5870.

[16]: Kittel, C. (2005). *Introduction to Solid State Physics 8th Ed.* John Wiley & Sons.

[17]: Retrieved from: Inorganic Crystal Structure Database (ICSD). Reference number 44328

[18]: Pierret, R.F. (2003) "*Advanced Semiconductor Fundamentals*" Volume VI, 2nd Ed. Pearson Education, Inc.

[19]: Pedrotti, F.L., Pedrotti, L.S. (1993) "*Introduction to Optics*" 2nd Ed. Prentice Hall.

[20]: *Optics: Reflection & Refraction*. (n.d.). Retrieved from http://www.capphysics.ca/PhysLab/Phys104/Optics%20reflection%20refraction/index.htm

[21]: PVeducation. (n.d.). *Light Generated Current*. Retrieved from http://pveducation.org/pvcdrom/solar-cell-operation/light-generated-current

[22]: Siegel, E. (2013, 07 12). *The Dark Depths of the Universe*. Retrieved from http://scienceblogs.com/startswithabang/2013/07/12/the-dark-depths-of-the-universe/

[23]: M.A.Green. (2003). Third Generation Photovoltaics. Springer.

[24]: Hecht, J. (n.d.). *Sophisticated optical designs help photovoltaics reach record efficiency*. Retrieved from http://www.renewableenergyworld.com/rea/news/article/2009/01/sophisticated-optical

[25]: R.W. Miles, K. H. (2005). Photovoltaic solar cells: An overview of state-of-the-art cell development and environmental issues. *Progress in Crystal Growth and Characterization*, 1-42.

[26]: *GaSb-Gallium Antimonide Basic Parmeters*. Retrieved from http://www.ioffe.ru/SVA/NSM/Semicond/GaSb/bandstr.html

[27]: T. M. Rossi, D. A. (1990). ptype doping of gallium antimonide grown by molecular beam epitaxy using silicon. *Journal of Applied Physics Letters*, 2256-2258.

[28]: Ohring, M. (2002). *Materials Science of Thin Films Deposition & Structure.* Academic Press.

[29]: Hu, C. C. (2009). *Modern Semiconductor Devices for Integrated Circuits.* Prentice Hall.

[30]: Retrieved from http://marriott.tistory.com/97

[31]: Walsh, L. a. (2010). Electrical Properties of Materials . Oxford University Press.

[32]: Adelaide, U. Retrieved from http://www.iga.adelaide.edu.au/workshops/ncgqhe.html

[33]: *Press Release: The 1998 Nobel Prize in Physics*. (n.d.). Retrieved from http://www.nobelprize.org/nobel_prizes/physics/laureates/1998/press.html.

[34]: Kakudo, N. K. (2005). X-Ray Diffractin by Macromolecules. Springer Series in Chemical Physics.

[35]: Retrieved from http://laserpointerforums.com/f44/make-your-own-laser-spectrometer-62605.html

[36]: Bader, R. F. (n.d.). *An Introduction to the Electronic Structure of Atoms and Molecules*. Retrieved from http://www.chemistry.mcmaster.ca/esam/Chapter_1/problems.html

[37]: Smith, B. C. (1996). Fudementals of Fourier Transform Infrared Spectrospcapy . CRC Press, Inc.

[38]: K. C. Cadien, A. H. (1981). Growth of singlecrystal metastable semiconducting (GaSb)1−xGex films. *Journal of Applied Physics Letters*, 773.

[39]: Greene, A. H. (1979). Growth and electrical properties of sputterdeposited singlecrystal GaSb Films on GaAs substrates. *Journal of Applied Physics Letters*, 6396.

[40]: A. SUBEKTI, V. W. (1996). OHMIC CONTACTS TO n-TYPE AND p-TYPE GaSb. *Solid-Stare Electronics*, 329.

[41]: J. Kujala, N. S. (2014). Native point defects in GaSb. *Journal of Applied Physics*, 116.

[42]: Ville Virkkala, V. H. (2012). Native point defect energetics in GaSb: Enabling p-type conductivity of undoped GaSb. *Journal of PHYSICAL REVIEW B*, 86.